CO_2 hydrate formation in coil heat exchangers

An experimental and theoretical study

C.B. Groen

January 23, 2012

Report number 2487

MSc Thesis

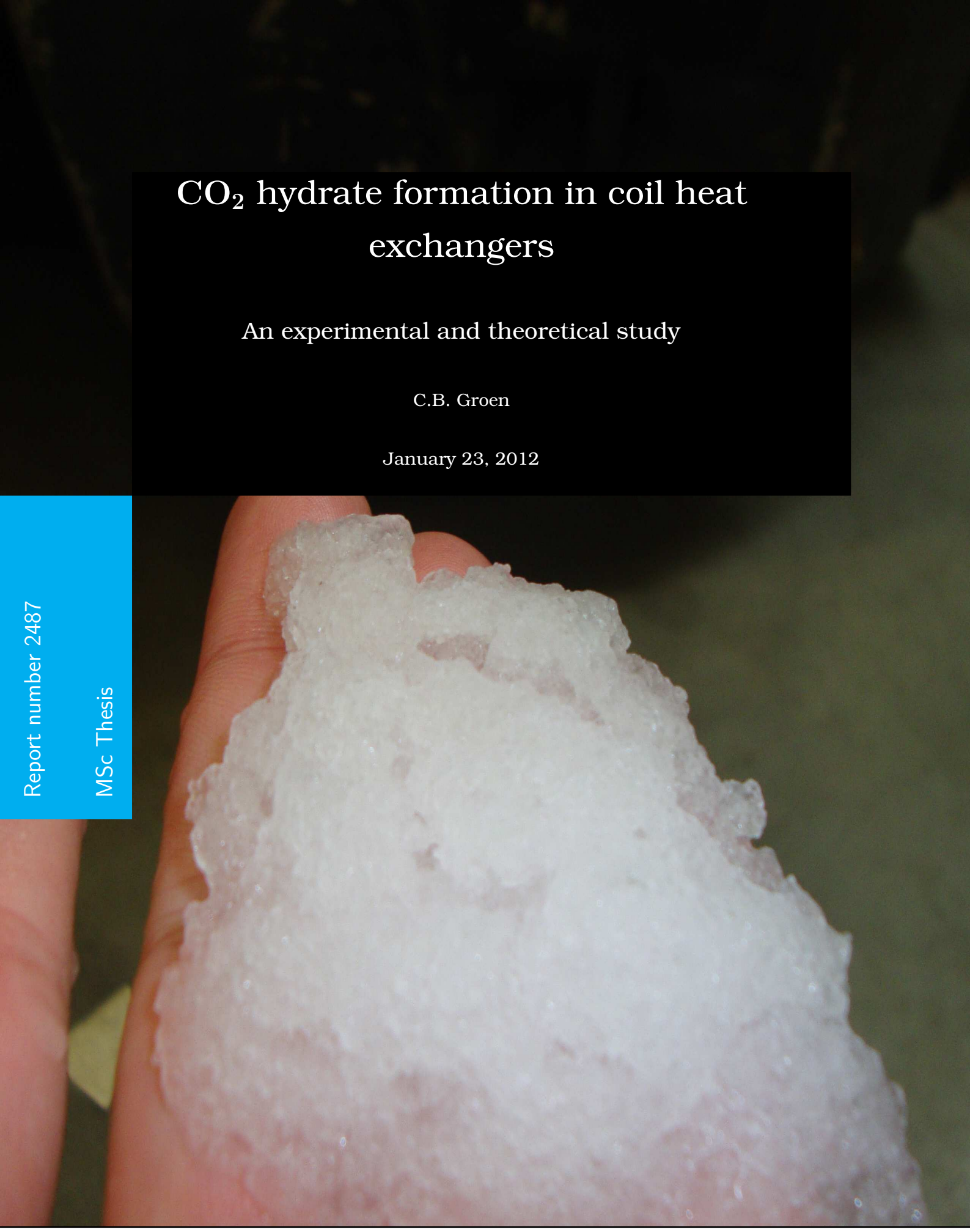

TU Delft Delft University of Technology

GROLLEMAN COLDSTORE

IBK GROEP

LUNENBURG

Sparkling Projects

CO_2 hydrate formation in coil heat exchangers

An experimental and theoretical study

Sustainable Processes and Energy Technologies
at
Delft University of Technology

Report number: 2487

C.B. Groen

January 23, 2012

Faculty of Mechanical, Maritime and Materials Engineering (3mE) · Delft University of Technology

Abstract

CO_2 hydrates are a crystalline structure of water molecules enclosing CO_2 molecules, formed in a stochastic process under the appropriate conditions of pressure and temperature. They are a possible replacement for conventional (synthetic) refrigerants that should be phased out for either legal, safety or environmental reasons. The main advantages of CO_2 hydrates are its formation conditions (phase change above 0 °C) and the enthalpy of dissolution (about 500 kJ/kg), which is higher than that of water ice (333 kJ/kg).

Aiming for a reduction of energy consumption, requiring more efficient processes, CO_2 hydrates have been proposed for rapid chilling of meat. Spraying the hydrates on the meat will extract thermal energy from it for the dissolution of the hydrates. Advantage of rapid cooling, besides the lower process time, is the decreasing dehydration of meat, resulting in less spoiling of meat. Besides cooling, the CO_2 gas has a conserving influence on meat, which might potentially increase the shelf life of meat.

An experimental set-up for continuous CO_2 hydrate production, which is designed and constructed during the present study, is presented. The system consists of two thermostatic baths and two coil heat exchangers, a gear pump and two buffer vessels. A saturated mixture of water and CO_2 is cooled at temperatures between 4 and 8 °C under hydrate forming conditions (10 to 40 bar). The experimental set-up includes temperature and pressure sensors and a Coriolis flow meter from Endress+Hauser, which enables the measurement of the density of the mixture.

To predict the hydrate slurry concentration produced by the experimental set-up, a growth model needs to be developed. A description of a suitable growth model is given by [Skovborg and Rasmussen, 1994], which is a simplification of the model from [Englezos et al., 1987]. In the present study, tools for this growth model are developed, being a thermodynamic model to predict the equilibrium pressure at a given temperature and the fugacity coefficients, which are used in a flash model to compute the mole fractions of the bulk phase. With these models the driving force for mass transfer can be quantified.

The thermodynamic model, needed for the growth model, is based on the Peng-Robinson-Stryjek-Vera equation of state combined with the Huron-Vidal-Orbey-Sandler mixing rules.

The Gibbs free energy is calculated with the UNIQUAC model. A procedure for the flash model, taking into account hydrate formation, is given by [Gupta et al., 1991].

The developed thermodynamic model and flash model are validated with data from literature or experimental data from the set-up. The equilibrium pressure is predicted in good agreement with experimental data from [Wendland et al., 1999] within a relative error of 4.42%. The bulk phase mole fraction of CO_2 in the liquid phase is compared with the solubility of CO_2 from [Diamond and Akinfiev, 2003]. At equilibrium conditions these are in good agreement, but in the hydrate-liquid region the mole fractions deviate. At supersaturated conditions with a driving force of 2 K, the relative error is between 4.2 and 8.0 %.

The mole fractions of CO_2 and H_2O in the liquid phase are used in the calculation of the solution density, which in turn is used in calculating the density of the hydrate slurry. As expected from the deviations in the the mole fractions, the solution density deviates from the experimental data once the mixture is supersaturated.

The experimental set-up produces hydrates and samples have been taken successfully, which can be used to perform experiments with meat in future research. The measurement of the density however does not show the increase reported in literature.

The thermodynamic model and the flash model can be used in the development of the growth model in future work. To be able to measure the density of the produced slurry from conducted experiments more accurately, some modification are proposed for the experimental set-up.

Table of Contents

List of Figures

List of Tables

Nomenclature

Symbols

a	Attractive volume parameter	$kg \cdot m^5 \cdot mole^{-2} \cdot s^-2$
A	Area	m^2
	Dimensionless attractive volume parameter for the mixture in section 3-2	
A_{g-l}	Gas liquid interfacial area	m^2
b	Excluded volume parameter	$m^3 \cdot mole^{-1}$
B	Dimensionless excluded volume parameter for the mixture in section 3-2	
C	Langmuir constant	Pa^{-1}
C^*	Molar volume dependent function for the PRSV equation of state	
c_p	Specific heat capacity	$J \cdot kg^{-1} \cdot K^{-1}$
C_p	Molar heat capacity	$J \cdot mole^{-1} \cdot K^{-1}$
C_w^0	Initial concentration of water	$mole \cdot m^{-3}$
d	Diameter	m
D	Variable in section 3-3, defined in equation 3-49	
f	Fugacity	Pa
g	Gravitational acceleration	$m \cdot s^{-2}$
δg	Variation of Gibbs free energy	
G	Gas	
G^E	Gibbs free energy	
h	Enthalpy	$J \cdot mole^{-1}$
	Convective heat transfer coefficient in section A-1	$W \cdot m^{-2} \cdot K^{-1}$
k_L	Mass transfer coefficient	$m \cdot s^{-1}$
k_w	Thermal conductivity	$W \cdot m^{-1} \cdot K^{-1}$
K	Equilibrium constant	
l	Parameter in UNIQUAC model	
L	Length	m
m	Mass	kg

M	Molar mass	$kg \cdot mole^{-1}$
n	Number of moles	$mole$
N_a	Avogadro constant	$mole^{-1}$
N_0	Number of empty hydrate lattices	
P	Pressure	Pa
q	Relative molecular surface area in section 3-2	
Q	Heat flow	W
r	Radius	m
	Relative molecular volume in section 3-2	
R	Gas constant	$J \cdot mole^{-1} \cdot K^{-1}$
s	Lattice dimension	m
T	Temperature	K or $^{\circ}C$
T_0	Reference temperature	K
u	Flow velocity	$m \cdot s^{-1}$
	Binary energy interaction parameter in section 3-2	$J \cdot mole^{-1}$
U	Overall heat transfer coefficient	$W \cdot m^{-2} \cdot K^{-1}$
V	Volume	m^3
	Specific volume in section 3-4	$m^3 \cdot kg^{-1}$
w	Mass fraction	
x	Mole fraction	
y	Mole fraction	
z	Length	m
	Lattice coordination number in section 3-2	
Z	Compressibility	

Greek symbols

α	Thermal diffusivity in appendix A	$m^2 \cdot s^{-1}$
β	Volumetric coefficient of thermal expansion	K^{-1}
	Phase fraction in section 3-5-2	
γ	Activity coefficient	
ϵ	Ratio of free large cavities and total free cavities	
θ	Cavity occupancy	
Θ	UNIQUAC surface fraction	
ϕ	Fugacity coefficient	
Φ	UNIQUAC volume fraction	
μ	Chemical potential	
	Dynamic viscosity in appendix A	$Pa \cdot s$
ν	Molar volume	$m^3 \cdot mole^{-1}$
	Cavity in section 3-2-2	
	Kinematic visocisty in section A-1	$m^2 \cdot s^{-1}$
π	Number of phases	
ρ	Density	$kg \cdot m^{-3}$
τ	Interaction parameter in the UNIQUAC equation	
σ	Surface tension	$N \cdot m^{-1}$
ω	Accentric factor	
Ω	Stability variable	

Subscripts

0	Reference conditions
b	Bath
	Bulk in chapter 3
c	Critical
eq	Equilibrium
exp	Experimental
G	Gas
H	Hydrate
i, j	Component (H_2O or CO_2)
k, m	Phase (L, V or H)
l	Large
L	Liquid
mix	Mixture
r	Reference phase
s	Small
	Surface in section 3-1
sol	Solution
tb	Turbidity point
v	Vapor
	Volume in section 3-1
w	Water

Superscripts

b	Bulk phase
H	Hydrate
int	Interface
l	Liquid
sat	Saturated
V	Vapor
β	Empty hydrate

Abbreviations

AAD	Average absolute deviation
AD	Absolute deviation
CSTR	Continuous stirred tank reactor
HVOS	Huron-Vidal-Orbey-Sandler
PRSV	Peng-Robinson-Stryjek-Vera
RD	Relative deviation

Dimensionless numbers

Nu	Nusselt number, defined in equation A-7	
Pr	Prandtl number	$\frac{C_p \cdot \mu}{k}$
Ra	Rayleigh number, defined in equation A-6	
Re	Reynolds number	$\frac{\rho \cdot u \cdot d}{\mu}$

Acknowledgements

This thesis does not only mark the end of my graduation project, but also of my life as a student. I met a lot of people who played an important role during this time, helped me to develop ideas and made this work possible. It is impossible to mention all of them here, but some I would like to thank in specific, not necessarily in order of importance.

First of all my parents, sisters and brother, who have endured my stubbornness since childhood (although not always without complaints) and always supported me. They form the basis I can always rely on.

Carlos, you were always available for questions and guided me through the process of the graduation project with care and eye for details. Catalina, thanks for your assistance during the project and persistence on the moments it was hard to convince me I did something wrong.

From IBK Groep: Jan and Henk, thanks for the pleasant cooperation during the construction of the experimental set-up. Wim, thanks for your assistance with practical issues during the first experiments in Houten.

All the people I met at the P&E department, especially the students that worked in office 32, made the time there unforgettable. You not only contributed to study related issues, but also the social coherence is something I really enjoyed. I hope we can continue to have some drinks and BBQ's occasionally.

Rob, we have worked together since the very first project of the Mechanical Engineering program and you contributed a lot to my development during these years. Much appreciated!

This thesis not only marks an end point, but also the start of something new. We will meet again!

Chapter 1

Introduction

Refrigeration accounts for about 15% of the energy consumption in industrialized countries. An alternative for reduction of the amount of the primary refrigerant in cooling systems is the transport of cold by a secondary refrigerant from a contained refrigeration machine. By injecting a gas like CO_2 in a cooled liquid, a two phase fluid can be produced without a mechanical process. When used as a (secondary) refrigerant, they are known to have a higher energy efficiency due to the additional latent heat of the solid phase in the mixture [Fournaison et al., 2004, Marinhas et al., 2006], compared to single phase fluids. This allows use of smaller quantities of the primary refrigerant and operation of the primary refrigerant in a contained environment.

Aiming for a reduction in energy consumption, requiring more efficient processes, CO_2 hydrates have been proposed for chilling of meat. Spraying the hydrates on the food will extract thermal energy from it for the dissolution of the hydrates. Besides cooling, the CO_2 gas has a conserving influence on meat, increasing the shelf life in supermarkets. Losses due to exceeding of the shell life is estimated to be 5%. Another advantage of rapid cooling is a decreased dehydration of meat, resulting in less spoiling of meat, which is estimated to be about 3% with the conventional cooling techniques. This project aims at a decrease of 50% of the spoiling of meat over the whole chain (slaughter house, transport, storage, supermarket), which would be 3.000.000 kg of meat at Lunenburg Vlees B.V., producting 60.000.000 kg annualy [Grolleman, 2010].

Not only the meat loss, but also the energy consumption of the cooling process is expected to decrease due to the better heat transfer from the hydrate slurry to meat, compared to the conventional cooling method (blowing cooled air over the meat).

To investigate the influence of direct cooling by CO_2-hydrates on meat, an experimental hydrate production set-up is developed at Delft University of Technology. The project is funded by "Koudegroep Delft/Wageningen", a cooperation of Wageningen Universtity and Delft University of Technology and a delegation from industry, among which Grolleman Cold Storage. The designed set-up is constructed by IBK Groep, an engineering company with focus on refrigeration techniques and installations.

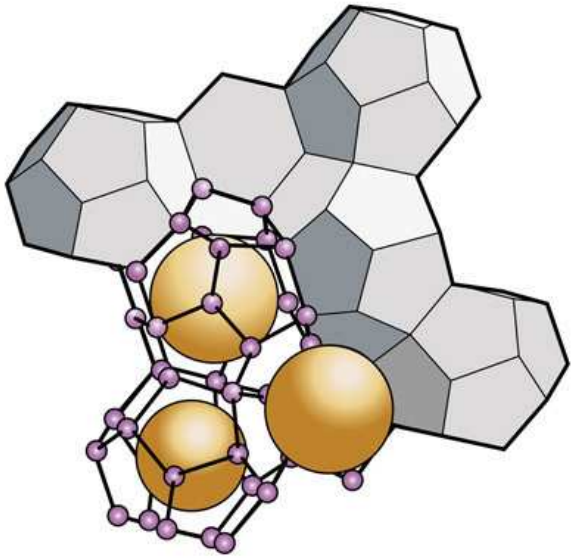

Figure 1-1: Visual representation of a hydrate lattice. Image by Lenny Martinez.)

With an eye on upscaling of the process in the future, a model is to be developed to predict the amount of hydrates in the set-up. Hydrate formation can be described with crystallization theory, including nucleation, growth and agglomeration [Sloan and Koh, 2008].

The first objective of the present study is to develop the tools for such a growth model, being a thermodynamic model to predict the equilibrium pressure for hydrate formation conditions at a given temperature and a flash model to distinguish the different phases (vapor, liquid and solid) in the hydrate slurry.

A theoretical background on hydrates and its properties is given in chapter 2. This chapter also describes the most important phenomena of hydrate formation and dissociation, including relevant models from literature.

The thermodynamic model and the flash model are described in chapter 3, which also includes a description of how the growth model can look like. The developed thermodynamic model and flash model are validated for equilibrium conditions, see section 3-5. With these tools, the growth model should predict the hydrate concentration in the hydrate slurry. From this concentration the slurry density can be determined, which can be compared with the measured slurry density in the set-up.

The second objective of this work is to test the constructed experimental set-up to see if hydrates can be produced and the density can be measured. The experimental set-up is described in chapter 4 and the results of these experiments are presented in section 4-3. As the purpose of this set-up is to cool meat and investigate the influence of meat on the CO_2 hydrates, an indication of the amount of hydrates required to cool a certain mass of meat is given in appendix A.

The conclusions from this study and recommendations for future work are presented in chapter 5.

Chapter 2

Theoretical background

In the gas industry hydrates have been treated for a long time only as an unwanted effect in transportation of natural gas, causing plugging of pipelines. Most effort was put in research aiming at prevention of the formation or decomposition of hydrates and as a result the thermodynamics of the hydrate formation process are quite well understood, in contradiction to hydrate formation kinetics. When hydrates appeared to be applicable in for example gas storage and CO_2 storage in the ocean [Chatti et al., 2005], research also started to focus on formation kinetics.

In this study a model is developed to predict the continuous formation of hydrates from a CO_2-water mixture, which will be used later for rapid cooling of meat. The phase diagram of this mixture depends on pressure and temperature as well as on the global mole fraction of CO_2 in the system. The flowing conditions of the mixtures are related to the (volume) fraction of hydrates dissolved in the solution.

In this chapter the properties of hydrates will be described briefly in section 2-1 and the hydrate formation process, which is divided into nucleation and growth, in section 2-2. Hydrate dissociation is mentioned briefly in section 2-3 but is not part of the present study. Finally the main differences between batch production of hydrates, which is the most common in literature, and continuous production are explained in section 2-4.

2-1 Hydrate properties

Clathrate hydrates or aqueous hydrates are non-stoichiometric compounds, consisting of a number of water molecules enclosing a guest molecule. The water molecules have no chemical bonding with the guest molecule. Three hydrate structures are known (sI, sII and sH), each with different arrangement of the water molecules and number of water molecules, resulting in different number and size of cavities available to host the guest gas molecules [Fournaison et al., 2004].

A polyhedron, forming a small cavity, is the fundamental hydrate unit that can be found in all structures. It has 12 pentagonal faces, indicated as 5^{12}, the base number referring to the

number of edges and the exponent to the number of faces. The large cavity in structure sI has 12 pentagonal and 2 hexagonal faces, referred to as $5^{12}6^2$. A sI unit cell consists of 46 water molecules and fits in a cube with edge lengths of 12 Å. For comparison, sII hydrate structures have 16 small cavities, formed by the same 5^{12} polyhedrons and 8 large cavities with 12 pentagonal and 4 hexagonal faces, referred to as $5^{12}6^4$. It consist of 136 water molecules and would fit in a cube with edges of 17.3 Å. In table 2-1 the cavity sizes and the number of cavities found in the different hydrate structures are listed.

Table 2-1: Properties of gas hydrate structures per unit cell. [a]

Structure	sI		sII		sH		
Cavity type	Small	Large	Small	Large	Small	Medium	Large
Description	5^{12}	$5^{12}6^2$	5^{12}	$5^{12}6^4$	5^{12}	$4^35^66^3$	$5^{12}6^8$
Number of cavities	2	6	16	8	3	2	1
Average cavity radius [Å]	3.95	4.33	3.91	4.73	3.94	4.04	5.79
Lattice dimension[b] [Å]	12		17.3		12.2		
Number of water molecules	46		136		34		

[a] Taken from [Sloan, 2000].
[b] Depending on temperature, pressure and guest composition.

The hydrate structure that is formed depends on the guest molecule and for a gas mixture on the composition of the gas mix. In a $CO_2 - N_2$ mixture for example, a mole fraction higher than 15% CO_2 results in structure sI hydrates, below 15 % in structure sII hydrates. Adding tetrahydrofuran (THF) to this mixture, will change sI into sII structures, increasing the amount of encapsuled guest molecules, which enhances the hydrate stability. Mixtures of sI and sII structures only exist in unusual circumstances [Davidson et al., 1987]. $H_2O - CO_2$ mixtures are reported to form structure I hydrates, with the CO_2 molecules occupying both the large and the small cavities of the hydrate [Munck et al., 1988].

The most important difference with "regular" ice, besides the crystal structure, is that hydrates do not form when there is no guest component of a proper size present, while ice forms as a pure component. The (mechanical) properties of hydrates are often very similar to the properties of ice, as hydrates typically are composed of between 85 % and 90% (mole fraction) of water.

The gas molecules entering the cavities stabilize the hydrate structure and at most one guest molecule can occupy a cavity. Which cavities are occupied depends on the size of the guest molecules. It is possible to form a hydrate with only the large cavities occupied, but filling only the small cavities will not form a stable hydrate. If the guest molecule fits in the small cavity, also the large cavities will be occupied. The cavity occupation can be described by a Langmuir-type equation.

The phase behavior of CO_2 hydrates is shown in figure 2-1 with the stable hydrate region bounded by the $H - L_{CO_2} - V_{CO_2}$, $H - I_w - V_{CO_2}$ and $H - L_w - L_{CO_2}$ lines. The CO_2 hydrate will be stable for any temperature as long as the pressure is higher or equal to the equilibrium pressure.

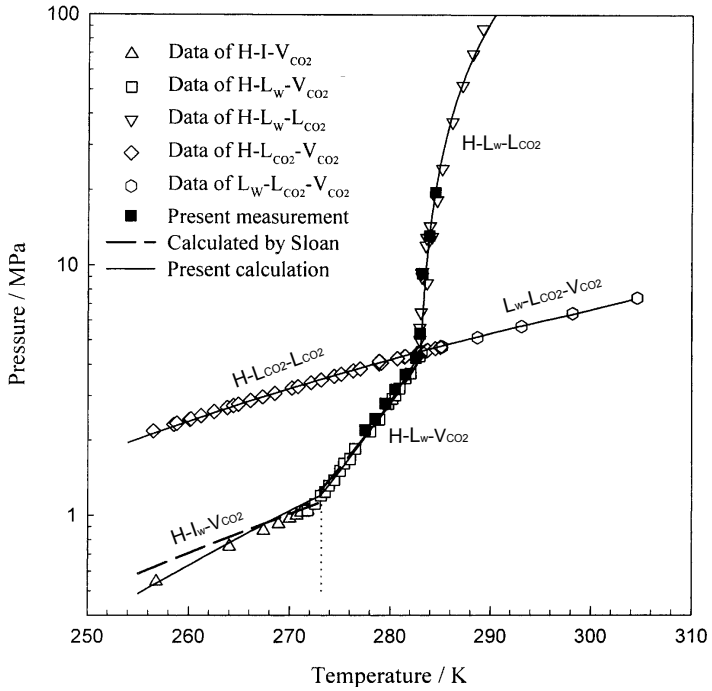

Figure 2-1: Phase diagram with three phase equilibrium lines for a $H_2O - CO_2$ mixture. Taken and modified from [Yang et al., 2000].

2-2 Hydrate formation

Hydrate formation is a stochastic phase change process and can be treated as a crystallization process, requiring supersaturated process conditions. Hydrate structures grow from the nuclei formed in the supersaturated solution, forming an interface with a variation of the Gibbs free energy. The formation process involves the formation of gas-water clusters and their growth to critical sized stable nuclei, resulting in the formation of a hydrate. When the gas-water clusters are (much) smaller than the critical size, the nuclei are unstable and may either grow or break in the aqueous solution [Bishnoi and Natarajan, 1996]. The amount of gas molecules dissolved in the solution and consumed in the hydrate phase during formation is illustrated in figure 2-2.

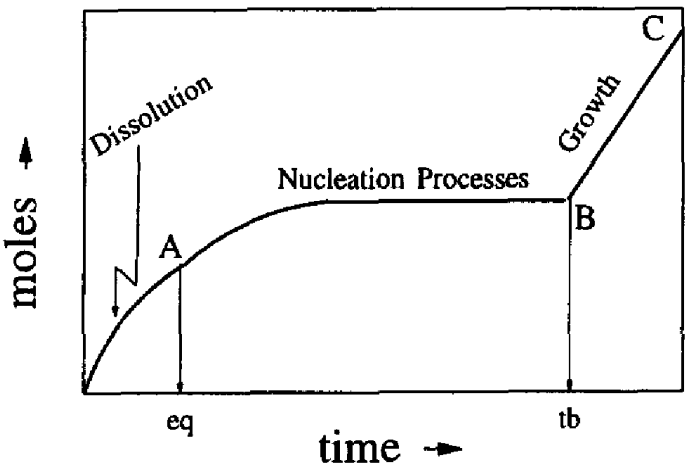

Figure 2-2: Typical gas consumption during hydrate formation. Before point A: dissolution of the gas in water, A to B: nucleation process, B to C: growth of hydrates. Point A is the equilibrium point at the system temperature and pressure, point B the turbidity point, from where the hydrates are visible. Figure taken from [Bishnoi and Natarajan, 1996].

Hydrate formation can be written in a general formula as

$$G + n_w H_2O \rightleftharpoons G \cdot n_w H_2O \tag{2-1}$$

with n_w the number of water molecules per unit cell and G a gas molecule, although in practice hydrates contain more water than predicted by the ideal composition, as occupation of all cavities would mean that a perfect crystal is formed [Sloan and Koh, 2008].

The hydrate formation process is similar to crystallization and can be described by distinguishing between nucleation (see subsection 2-2-1) and growth of the nuclei (subsection 2-2-2).

2-2-1 Hydrate nucleation

Hydrate nucleation is based on its driving force, defined as the chemical potential difference between the old phase and the new phase, also called supersaturation [Ribeiro Jr and Lage, 2008], see equation 2-2.

Several forms of this definition have been proposed for the driving force of hydrate nucleation: the difference of chemical potential of water in the liquid water phase and the hydrate phase [Skovborg and Rasmussen, 1994], fugacity difference of the guest molecule at equilibrium conditions and the operating conditions [Natarajan et al., 1994] and the difference between the operating temperature and the equilibrium temperature for hydrate formation [Vysniauskas and Bishnoi, 1983]. [Sloan and Koh, 2008] demonstrated that these definitions can all be defined as the variation of the Gibbs free energy of the system.

$$\Delta g = \mu_G + n_w \mu_w - \mu_H \tag{2-2}$$

A thermodynamic model is required to compute the chemical potential of water in the hydrate phase and the the model proposed by [Van Der Waals and Platteeuw, 1959a] is used in most studies.

Hydrate kinetics on molecular level are described assuming the nuclei are spherical and the interface of the gas-liquid phases is sharp, where in real life a diffuse region will exist where the properties vary between the values of the individual phases. With this last assumption the properties of the phases are taken as in the bulk phases. It is reported by [Ribeiro Jr and Lage, 2008] that this is valid when the thickness of the interfacial region is smaller than the critical radius of the hydrates.

The alternative would be a much more complex dynamic molecular model to predict accurate properties for the phase field theory [Kvamme et al., 2004].

An interesting phenomenon of hydrate formation is the so called "memory effect": a water gas mixture in which hydrates were present before will form hydrates more easily than from a water-gas mixture with no hydrate formation history [Takeya et al., 2000]. Two hypothesis can be found in literature to explain this effect, either a residual hydrate structure remains in the solution which is above dissociation temperature, or the dissolved gas from the hydrates remains in the solution. Neither has been proved so far. The memory effect however does imply that repeating temperature cycles will decrease the formation time.

The stochastic nature of the induction time of hydrate formation decreases with increasing driving force, and also depends on factors like the cooling rate or even the apparatus in which the hydrates are produced, making it very difficult to predict exactly when the first hydrate nuclei will be present in the solution.

2-2-2 Hydrate growth

Hydrates contain up to 15% gas and as the solubility of that gas in water is usually lower (for CO_2 at hydrate equilibrium conditions between 1.5 and 3 %), mass transport of the gas molecules to the hydrate surface plays an important role in in the growth process. Besides mass transport, the growth kinetics and the heat transfer of the exothermic growth process from the crystal surface to the solution is important, although it is not clear which phenomena is dominant.

Hydrate growth is described in numerous ways, as shown by [Ribeiro Jr and Lage, 2008], reporting to have found 14 different hydrate growth models in literature. The majority of these models is only valid for specific operation conditions, are applicable to a specific process or depend on a lot of fitting parameters and will not be discussed here. Three models are potentially suitable for this study:

1. **Englezos-Kalogerakis-Dholabhai-Bishnoi**

   In this model [Englezos et al., 1987], developed to describe data obtained from experiments, crystallization theory is combined with mass transfer at the gas-liquid interface. The driving force in this model is the difference of the fugacity of the dissolved gas and the three-phase equilibrium fugacity. The model contains two parameters that have to be fitted with experimental data (α_2, an empirical parameter and K^*, a kinetic resistance constant). [Chun and Lee, 1996] report a good agreement of this model, for formation of CO_2 hydrates, with experimental data for the initial states, but an increasing systematic deviation for longer operation times. The model is also reported to be sensitive to the experimental determined number of moles consumed up to the turbidity point (turbidity is a qualitative characteristic of a liquid sample in which light is scattered by solid particles). [Skovborg and Rasmussen, 1994] noted that the gas consumption rate during hydrate growth is predicted to increase with increasing operation time, in contradiction to experimental observations. According to [Clarke and Bishnoi, 2005] the model is only valid for low supersaturation conditions. An inconsistency in the driving force is reported by [Sloan and Koh, 2008].

2. **Skovborg-Rasmussen**

   [Skovborg and Rasmussen, 1994] proposed a simplified model based on the model of [Englezos et al., 1987], assuming that all resistance to mass transfer during hydrate formation lays in the diffusion of the dissolved gas from the gas-liquid interface to the liquid bulk. With this assumption the population balance equation can be removed from the model. The model has been applied in simulation of natural gas hydrate formation by [Gnanendran and Amin, 2004], but they failed in obtaining convergence in the flash calculation, used to determine the amount of hydrates formed in the reactor.

3. **Herri-Pic-Gruy-Cournil**

   [Herri et al., 1999] claim that the kinetics of hydrate formation at the gas-liquid interface must be described by the crystalization theory and should include the population balance equation. The model includes both the nucleation and the growth of the hydrate formation process. The assumption of instantaneous, homogeneous nucleation used in the model of [Englezos et al., 1987], which is in contradiction with experimental observation, is removed from the model.

All described models are developed for (semi-)batch processes and use coefficients that have to be determined experimentally, so no entirely theoretical model is available. [Ribeiro Jr and Lage, 2008] conclude that hydrate formation kinetics should be described as a coupled heat and mass transfer problem and should include a population balance equation with models for breakage and agglomeration.

However, according to [Hoffmann, 2011], if only the amount of hydrates at the outlet of the generator have to be predicted, as in this present study, no population balance equation is needed.

2-2-3 Heat transfer

During the hydrate formation process the fluid transitions from two-phase to three-phase regime (gas-liquid-solid). At the same time the hydrate heat of formation has to be continuously removed to promote additional hydrate formation. Different flow regimes will occur along the path of hydrate formation in a continuous process, requiring different relations for the prediction of thermal and transport properties.

Plugging can be a problem in small pipe diameters. Heat transfer efficiency might be influenced by the flow pattern (changing slurry concentration, with changing parts of the tube wall exposed to the lower conductivity gas phase), the liquid layer might be critical. Turbulent flow, beneficial for the formation of hydrates, will require higher fluid velocities for increasing slurry concentration. For long pipe lengths this might increase the frictional heating significant, due to the fluid-wall drag. For small pipe lengths this can be ignored [Yang et al., 2008].

A high gas volume fraction will result in a high impact of the thermal conductivity of the carrier gas on the heat transfer rate at the process fluid side [Yang et al., 2008]. Hydrate formation kinetics will be favorable with vigorous mixing and hydrate formation will become heat transfer limited [Spencer and North, 1996].

2-3 Hydrate dissociation

Hydrate decomposition is driven by the difference between the equilibrium fugacity and the vapor fugacity of the gas phase, $f_{eq} - f_G^V$. The crystal hydrogen bonds account for about 80% of the enthalpy of dissociation of a hydrate and the heat of dissociation thus changes with changing cavitiy occupation [Sloan and Fleyfel, 1992]. It is expected that an increase of guest molecules in the cavities renders the hydrate structure loose, decreasing the enthalpy of dissociation [Kang et al., 2001].

[Delahaye et al., 2005] use the Clausius-Clapeyron equation to calculate the dissociation enthalpy, in which it is represented as the slope of the equilibrium line in a logarithmic $P - \frac{1}{T}$ plot. Research of [Glew, 1959], [Barrer, 1959] and [Van Der Waals and Platteeuw, 1959a] showed that this equation is only valid for an invariant system with an (almost) constant temperature and within three restrictions:

1. The fractional guest occupancy of each cavity should not change.
2. The condensed phase volume should be negligible compared to the gas volume.
3. The gas composition should be constant.

Determining the heat of dissociation, the existence of (water) ice in the mixture has to be considered, as not all water might be converted into hydrates [Kang et al., 2001]. [Marinhas et al., 2006] determined the dissociation enthalpy by differential scanning calorimetry measurements to be approximately 500 kJ/kg, which is higher than the dissociation enthalpy of ice (333 kJ/kg).

2-3-1 Heat transfer

Heat transfer during decomposition of the hydrates is analogous to nucleate boiling and is suggested to consist of two steps. The first step is the destruction of the clathrate host lattice, followed by the desorption of the gas molecule from the surface [Bishnoi and Natarajan, 1996]. [Kim et al., 1987] assumed the hydrate to be surrounded by a cloud of gas in a kinetic decomposition model.

2-4 Batch and continuous hydrate production

During hydrate formation CO_2 is consumed from the saturated $H_2O - CO_2$ solution into the hydrate phase. This causes a pressure drop when a fixed volume like a tank reactor is used for hydrate formation, as the CO_2 in the gas phase replaces the CO_2 molecules consumed by the hydrates, see figure 2-3 for an example.

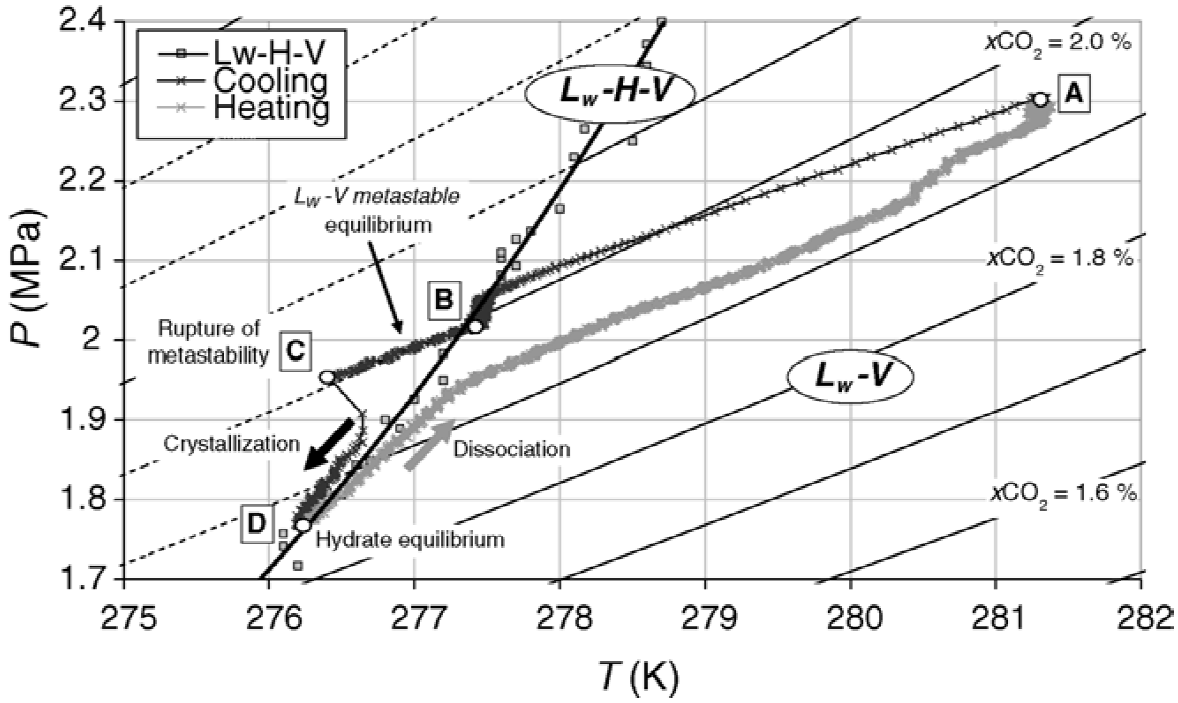

Figure 2-3: CO_2 hydrate formation and dissociation cycle with the iso-CO_2 lines representing the mole fraction of CO_2 dissolved in liquid water. Taken from [Marinhas et al., 2006].

In a continuous production either gaseous CO_2 is continuously fed to the system or there is an excess of CO_2 present, keeping the system at (almost) constant pressure. So, in contradiction to the described batch experiments and the formation process shown in figure 2-3, the mixture will not follow the iso-CO_2 concentration lines.

Most studies in literature on hydrate formation use a batch production, investigating either equilibrium conditions or the turbidity point. Some studies on continuous hydrate production have been identified.

[Gudmundsson et al., 2000] describes an experimental set up for the continuous production of natural gas hydrates in a CSTR reactor, including instrumentation and measuring considerations. In operation since 1997, some practical issues are reported concerning operation of the system. Two positive displacement pumps were used for mixing and circulation, causing pressure fluctuations in the systems due to the pulsating nature of the pumps, making it impossible to do accurate pressure drop calculations. The positive displacement pump used for circulation is replace by a variable speed high-pressure centrifugal pump.

For constant pressure operation, gas was injected at a higher rate than the consumption rate and the excess vented off through a gas flow meter, measuring the difference between the

amount of injected and vented gas to determine the consumed amount of gas. Plugging was observed sometimes in small diameter pipes (1/4 inch), which could be prevented by band heaters on that tube.

The project showed a higher consumption rate of gas during hydrate formation with increasing gas injection rate at a given temperature. Also, a decreasing temperature at a given gas injection rate resulted in a higher gas consumption.

[Hu et al.], [Hu et al., 2010] and [Hu et al., 2011] describe several experiments with a double tube heat exchanger in which hydrates are formed and dissolved in one of the tubes and a refrigerant flows in the other tube. The refrigerant is cooled by two chillers and a high pressure pump circulates the test fluid in the secondary tube. CO_2 is injected from a bottle into this circuit with the test fluid. Mass flow, temperature and pressure are measured at several locations. In the set-up mechanical properties like density, viscosity and heat of dissociation are investigated.

[Delahaye et al., 2008] and [Marinhas et al., 2006] describe various experiments with a loop consisting of a 220-type Micro pump, temperature and pressure sensors. CO_2 is injected in the flow by a syringe pump, connected to a CO_2 bottle. The loop is used to study formation and dissociation conditions and several temperature slopes and plateaus are applied to the loop.

Also some patents on continuous hydrate formation [Spencer and North, 1996, Heinemann et al., 2000] have been identified, dealing with gas hydrate formation processes.

Chapter 3

Model

To predict the solid mass fraction of hydrates in the slurry, produced in a coil heat exchanger, a hydrate growth model is to be developed. In this study the tools are developed to implement such a growth model in future work. To investigate what is required for this model, the procedure of a suitable growth model is described in section 3-1. The proposed growth model requires knowledge of the mole fractions in the three phases, which can be determined from a flash calculation. The flash model uses the fugacity coefficients, which are calculated in a thermodynamic model. This thermodynamic model also provides the equilibrium pressure at the experimental temperature. These models are developed in the present study, the thermodynamic model is described in section 3-2 and the flash calculation in section 3-3.

3-1 Growth model

In this section a procedure for the modeling of hydrate growth is given. It is intended to identify what models have to be developed before such a growth model can be implemented in future work. The growth of the formed hydrates be can described by a simplification of the model from [Englezos et al., 1987], proposed by [Skovborg and Rasmussen, 1994]. This simplified model assumes that the transport of gas molecules from the gas phase to the liquid phase is the rate-determining step in the hydrate formation process. Hydrate formation is described by a three-step process in this model:

1. Gas is transported from the bulk of the gas phase to the liquid bulk phase.
2. Gas diffusion to the hydrate-liquid interface from the bulk water phase and liquid film.
3. Adsorption of the gas molecules into the cavities of the hydrate structure.

The model assumes that the heat resistance around the particle is negligible and the reaction rate is high compared to the rate of gas transport to the reaction site, implying that hydrate

formation occurs at experimental temperature and the corresponding pressure that is available from a thermodynamic equilibrium model, as described in section 3-2.

The model also assumes that there is no secondary nucleation, which means all particles have the same size and grow at the same rate at any time, as the initial particle radius is set as the critical radius. The critical radius is the minimum radius a nucleus must have in order not to dissolve once it is formed. According to [Englezos et al., 1987], this means that the population balance can be replaced by a simple relation between the total surface of the particles and the amount of gas consumed in the formation process.

The amount of CO_2 dissolved in water at the turbidity point (n_{tb}), which is the first point where hydrates visually can be observed, should be larger than the amount of CO_2 at equilibrium conditions. This means that a state of supersaturation is required in order to prevent obtaining a negative number of particles from the model. The model is reported to be very sensitive to the initial value of n_{tb}.

The simplified growth model of [Englezos et al., 1987] is based on 3 assumptions:

- The water bulk phase is in equilibrium with some dissolved gas and the hydrate particles.
- At the gas-water interface, these two phases are in equilibrium.
- Gas transport from the gas-water interface to the bulk water phase occurs according to a simple film theory.

The growth model can be described in 7 steps:

1. Start with the given amount of water and CO_2, assuming $x_{CO_2} = 0$ and $x_{H_2O} = 1$.
2. Calculate the mole fraction of CO_2 dissolved in the liquid water phase at the water-gas interface in equilibrium with the gas phase, $x^{int}_{CO_2}$, using a thermodynamic (equilibrium) model, see section 3-2.
3. Calculate the driving force, defined as the difference between the mole fraction CO_2 dissolved at the interface and in the bulk water phase.

$$x^{int}_{CO_2} - x^{b}_{CO_2} \tag{3-1}$$

4. Calculate the gas consumption from

$$\frac{dn}{dz} = k_L \cdot \frac{A_{g-l}}{u} \cdot C^0_w \cdot (x^{int}_{CO_2} - x^{b}_{CO_2}) \tag{3-2}$$

5. Consider a finite element of length Δz and calculate the amount of CO_2 consumed in this element by

$$\Delta n = \frac{dn}{dz} \Delta z \tag{3-3}$$

6. Calculate the auxiliary bulk water phase composition by

$$x^b_{H_2O} = 1 - x^b_{CO_2} \tag{3-4}$$

7. Flash the auxiliary bulk water phase composition to calculate the new bulk water phase composition and a new amount of liquid water. A flash calculation procedure accounting for all three phases is proposed by [Gupta et al., 1991], see section 3-3.

Hydrates will only form when a sufficiently high concentration of CO_2 is present in the water phase. Until then, the amount of water in the bulk water phase will not change. As only one hydrate forming component (CO_2) is present, the driving force from this point on will be constant, under the conditions that the temperature and the pressure will not change. In the present study, the released heat of formation is constantly removed and the pressure drop is negligible due to the excess of CO_2 in the system. This is not the case in a batch reactor, see figure 2-3.

In the described procedure, the time steps dt and Δt in the model of [Skovborg and Rasmussen, 1994] are replaced by spatial steps dz and Δz as the flow velocity in the present study implicitly incorporates the time steps, while the model of [Skovborg and Rasmussen, 1994] describes a semi-batch tank reactor.

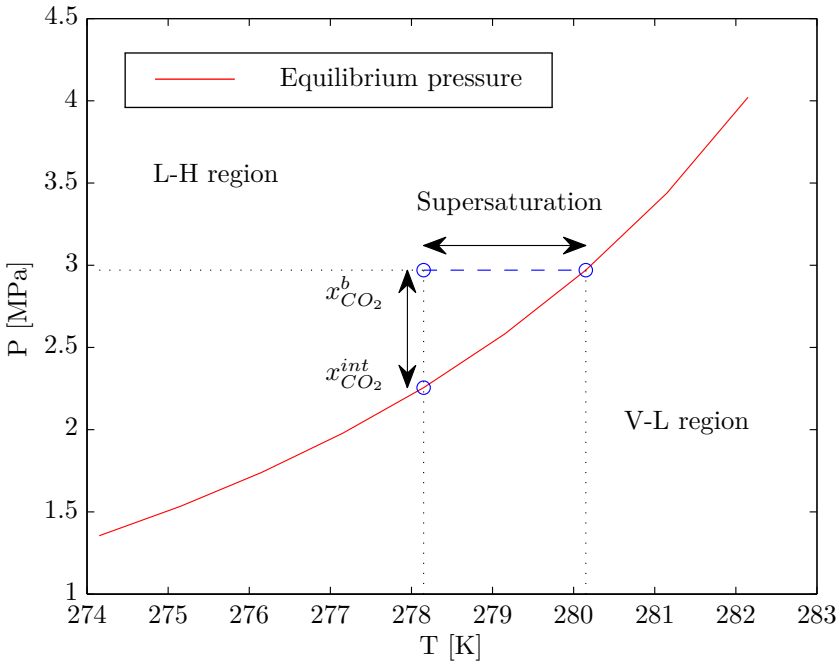

Figure 3-1: Supersaturation of the hydrate forming mixture at a fixed pressure and temperature. V-L = vapor - liquid, L-H = liquid-hydrate.

The interfacial area A_{g-l} can be assumed to be equal to the surface area of a spherical nucleus with critical radius r_c

$$A_{g-l} = 4 \cdot \pi \cdot r_c^2. \tag{3-5}$$

The critical radius is the radius at which the Gibbs free energy of the system reaches a maximum. The Gibbs free energy of the system ΔG is equal to the sum of the surface excess free energy ΔG_s (dissolved molecules becoming part of the surface of the nucleus) and the volume excess free energy ΔG_v (the molecules ending up in the interior of the nucleus). These two components of the Gibbs free energy of the system have opposite signs. ΔG_s scales with the square of the radius of the formed cluster, ΔG_v with the cube of the cluster radius. At the critical radius of the nucleus, the Gibbs free energy of the system is at a maximum, see figure 3-2. The molecules in the interfacial region always have a higher energy than those in the bulk phase, so the formation of a new phase requires a positive variation of the Gibbs free energy.

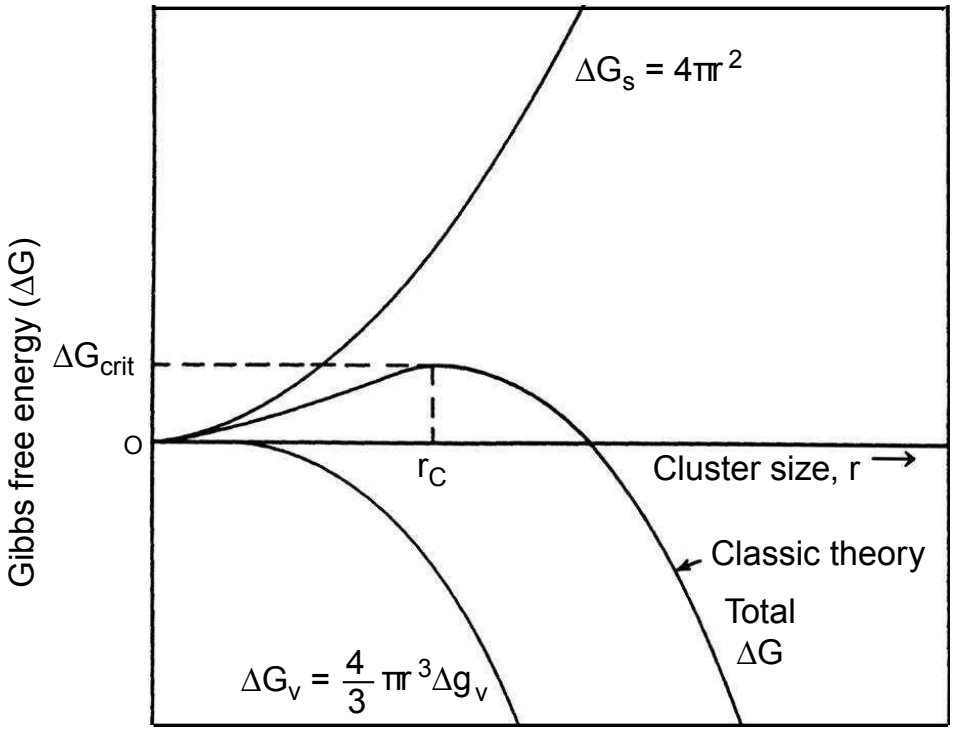

Figure 3-2: Comparison of surface excess free energy ΔG_s and volume excess free energy ΔG_v as a function of the cluster size. Taken from [Sloan and Koh, 2008].

The critical radius is derived as

$$r_c = \frac{-2\sigma}{\Delta g_v} \tag{3-6}$$

with σ the surface tension of ice in water.

[Englezos et al., 1987] and [Englezos and Bishnoi, 1988] give an expression for the Gibbs free energy per unit volume of formed hydrate

$$-\Delta g_v = \frac{R \cdot T}{\nu_H} \left(\sum_{j=1}^{2} \theta_j \cdot \ln \left(\frac{f_{b,j}}{f_{eq,j}} \right) + \frac{n_w \cdot \nu_w \cdot (P - P_{eq})}{R \cdot T} \right) \tag{3-7}$$

As an illustration of the order of magnitude of r_c, they calculate the critical radius for methane to be 30 - 170 Å, using equation 3-6 and 3-7.

As hydrate nucleation is not considered, the amount of initial nuclei is assumed to be equal to the amount of hydrates calculated from the flash calculation. In this case no secondary nucleation takes place, which means from that point on, no new nuclei are formed and only the existing nuclei grow.

The mole fraction at the gas-liquid interface $x_{CO_2}^{int}$ has to be calculated from the equilibrium conditions with a thermodynamic model, which is presented in section 3-2-3. The mole fraction of CO_2 dissolved in the bulk water phase, is then to be determined with a flash model, that uses the equilibrium pressure from the thermodynamic model at a lower temperature. The flash model is presented in section 3-3.

3-2 Thermodynamic model

The thermodynamic model for a $H_2O - CO_2 - THF$ mixture developed by [Sabil, 2009] and [Hartono, 2011] is adjusted and improved for a $H_2O - CO_2$ system.

The thermodynamic properties of the mixture are used to determine the equilibrium pressure at a given temperature. For this pressure, the fugacity coefficients in supersaturated conditions in the bulk phase (at a temperature lower than the saturated temperature), and at the interface (at the equilibrium pressure that corresponds with the temperature of the supersaturated bulk phase) are determined. See figure 3-1 for a visual representation.

The fugacity coefficients are later on used in a flash model to calculate the composition of the $H_2O - CO_2$ mixture (see section 3-3), which is required for the hydrate growth model.

The modeling procedure of the fugacities of the fluid phases (vapor and liquid) are different from the hydrate phase and are treated separately in subsections 3-2-1 and 3-2-2. The requirements for the thermodynamic three phase equilibrium, a special case of the thermodynamic model, are described in section 3-2-3.

3-2-1 Fluid phases

The Peng-Robinson-Stryjek-Vera (PRSV) equation of state is used for the fluid phases to describe the relation between the state variables pressure, temperature and volume.

$$P = \frac{R \cdot T}{V - b} - \frac{a}{V^2 + 2 \cdot b \cdot V - b^2} \tag{3-8}$$

For each component i, the attractive volume parameter a and the excluded volume parameter b can be calculated as

$$a_i = 0.457235 \frac{R^2 \cdot T_{c,i}^2}{P_{c,i}} \alpha_i \tag{3-9}$$

$$b_i = 0.077796 \frac{R \cdot T_{c,i}}{P_{c,i}} \tag{3-10}$$

with the Stryjek-Vera temperature dependency α_i as

$$\alpha_i = \left[1 + \kappa_i \cdot \left(1 - \sqrt{\frac{T}{T_{c,i}}} \right) \right]^2 \tag{3-11}$$

in which

$$\kappa_i = \kappa_{0,i} + \kappa_{1,i} \cdot \left(1 + \sqrt{\frac{T}{T_{c,i}}} \right) \left(0.7 - \frac{T}{T_{c,i}} \right) \tag{3-12}$$

$$\kappa_{0,i} = 0.378893 + 1.4897153 \cdot \omega, i - 0.17131848 \cdot \omega_i^2 + 0.0196554 \cdot \omega_i^3 \tag{3-13}$$

The pure component parameters for equations 3-10, 3-11, 3-13 and 3-14 are taken from [Lazzaroni et al., 2004] and listed in table 3-1.

Table 3-1: Pure component parameters for the PRSV equation of state, taken from [Lazzaroni et al., 2004].

	$T_c\,[K]$	$P_c\,[bar]$	ω	$\kappa_{1,i}$	r	q
CO_2	304.21	73.6	0.2250	0.04285	1.299	1.292
H_2O	647.13	220.55	0.3438	-0.06635	0.920	1.400

Using the UNIQUAC model, the Gibbs free energy can be calculated from

$$\frac{G^E}{R \cdot T} = \sum_i^n x_i \ln\left(\frac{\Phi_i}{x_i}\right) + \frac{z}{2}\sum_i^n q_i \cdot x_i \ln\left(\frac{\Theta_i}{\Phi_i}\right) - \sum_i^n q_i \cdot x_i \cdot \ln\left(\sum_j^n \Theta_j \cdot \tau_{ji}\right) \tag{3-14}$$

with the volume fraction

$$\Phi_i = \frac{r_i \cdot x_i}{\sum_j^n r_j \cdot x_j}\,, \tag{3-15}$$

and the surface fraction defined as

$$\Theta_i = \frac{q_i \cdot x_i}{\sum_j^n q_j \cdot x_j}\,. \tag{3-16}$$

The molecular Van der Waals volume r_i and molecular surface area q_i are given in table 3-1. The lattice coordination number z is equal to 10 and the temperature dependent interaction parameters τ_{ij} are defined as

$$\tau_{ji} = exp\left(-\frac{u_{ij}}{R \cdot T}\right) \tag{3-17}$$

with the binary energy parameters u_{ij} regressed from the equilibrium fugacities. This is done by fitting the model to experimental data from [Wendland et al., 1999] and [Adisasmito et al., 1991], as described in section 3-5-1. By definition $\tau_{ii} = \tau_{jj} = 1$. The first order polynomial fits for u_{ij} are given in table 3-2.

Table 3-2: Binary energy parameters in [J/mol] and with T in [K], regressed from experimental equilibrium data.

$u_{CO_2-H_2O}$	$-55720 + 279.82 \cdot T$
$u_{H_2O-CO_2}$	$-19599 + 78.13 \cdot T$

The model developed by [Sabil, 2009] iterates for the fugacities of water in the liquid phase and the hydrate phase, which converged in his model. However, the fugacity of the vapor phase showed large deviations, which appeared to be caused by the use of incorrect energy parameters u_{ij}. [Sabil, 2009] extrapolated these from data given by [Lazzaroni et al., 2004] in a temperature range of 298 to 333 K with help of a second order polynomial, using it in

the temperature range of 274 to 282 K. The values given in table 3-2 result in the correct prediction of vapor phase fugacity, required for the flash calculation.

Now the activity coefficient can be expressed as

$$\ln(\gamma_i) = \ln\left(\frac{\Phi_i}{x_i}\right) + \frac{z}{2} q_i \ln\left(\frac{\Theta_i}{\Phi_i}\right) + l_i - \frac{\Phi_i}{x_i}\sum_j^n (x_j \cdot l_j) - q_i \cdot \ln\left(\sum_j^n \Theta_j \cdot \tau_{ji}\right) + q_i - q_i \sum_j^n \frac{\Theta_j \cdot \tau_{ij}}{\sum_k^n \Theta_k \cdot \tau_{kj}}. \tag{3-18}$$

with the interaction parameters τ_{ij} from equation 3-17 and

$$l_i = \frac{z}{2}(r_i - q_i) - (r_i - 1)\ . \tag{3-19}$$

Using the Huron-Vidal-Orbey-Sandler (HVOS) mixing rule for multicomponent systems, the mixture parameters a_{mix} and b_{mix} can be calculated by

$$a_{mix} = b_{mix} \cdot R \cdot T \left[\sum_i x_i \frac{a_i}{b_i \cdot R \cdot T} + \frac{1}{C^*}\left(\frac{G^E}{R \cdot T} + \sum_i x_i \cdot \ln\left(\frac{b_{mix}}{b_i}\right)\right)\right] \tag{3-20}$$

and

$$b_{mix} = \sum x_i \cdot b_i. \tag{3-21}$$

The molar volume dependent function C^* in equation 3-20 is specific for an equation of state and for the PRSV equation of state C^* equal to -0.623225.

The parameters a_{mix} and b_{mix} can be written in their dimensionless forms

$$A = \frac{a_{mix} \cdot P}{R^2 \cdot T^2} \tag{3-22}$$

and

$$B = \frac{b_{mix} \cdot P}{R \cdot T} \tag{3-23}$$

and are used to calculate the compressibility factor, which can be expressed by rearranging equation 3-8 as

$$Z^3 - (1 - B) \cdot Z^2 + \left(A - 3B^2 - 2B\right) \cdot Z - \left(A \cdot B - B^2 - B^3\right) = 0. \tag{3-24}$$

The smallest real root of equation 3-24 is the liquid phase compressibility, the largest real root the vapor phase compressibility. The roots are found using the Matlab function "roots", which calculates the roots of a polynomial function from a vector with its coefficients.

The fugacity coefficient of both components in the fluid phases are calculated using an equation from [Orbey and Sandler, 1995],

$$\begin{aligned}\ln(\phi_i) &= \frac{b_i}{b_{mix}}(Z-1) - \ln(Z-B) - \\ &\frac{1}{2\sqrt{2}}\left[\frac{a_i}{b_i \cdot R \cdot T} + \frac{\ln(\gamma_i)}{C^*} + \frac{1}{C^*}\ln\left(\frac{b_{mix}}{b_i}\right) + \frac{1}{C^*}\ln\left(\frac{b_i}{b_{mix}} - 1\right)\right] \cdot \\ &\ln\left(\frac{Z + \left(1+\sqrt{2}\right)B}{Z + \left(1-\sqrt{2}\right)B}\right). \end{aligned} \tag{3-25}$$

The fugacity can than be calculated by

$$f_i = P \cdot \phi_i \cdot x_i. \tag{3-26}$$

The vapor liquid equilibrium composition is calculated using

$$K_{eq,i} = \frac{\phi_{l,i}}{\phi_{v,i}} \tag{3-27}$$

from which the vapor mole fraction of component i can be calculated for a given liquid mole fraction.

$$y_i = x_i \cdot K_{eq,i} \tag{3-28}$$

3-2-2 Hydrate phase

Unlike the thermodynamic properties of the fluid phases, H_2O and CO_2 require a different approach in the hydrate phase.

Water

The chemical potential of water in the hydrate phase is described by model from [Van Der Waals and Platteeuw, 1959b]:

$$\Delta\mu_w^{\beta-H} = -R \cdot T \sum_m v_m \cdot \ln\left(1 - \sum_j \theta_{mj}\right) \tag{3-29}$$

in which β refers to the empty hydrate lattice. The occupancy of cavity type m (either small or large) by component j, θ_{mj}, in equation 3-29 can be described by a Langmuir type equation

$$\theta_{mj} = \frac{C_{mj} \cdot f_j}{1 + \sum_k C_{mk} \cdot f_k} \tag{3-30}$$

with the Langmuir constant

$$C_{mj} = \frac{A_{mj}}{T} \cdot exp\left(\frac{B_{mj}}{T}\right). \tag{3-31}$$

As only CO_2 occupies the cavities in these hydrates, $j = CO_2$ and $C_{mj} = C_m$ and $f_k^V = f_{CO_2}^V$, which can be obtained from equation 3-26. The constants A_m and B_m in equation 3-31 are given in table 3-3.

Table 3-3: Langmuir constants for structure I CO_2 hydrates in equation 3-31, taken from [Parrish and Prausnitz, 1972].

	Small cavity	Large cavity
A [K/Pa]	$2.44 \cdot 10^{-9}$	$4.19 \cdot 10^{-7}$
B [K]	3410	2813

With the constants given by [Munck et al., 1988] (see table 3-4) and with $T_0 = 273.15\,K$, the chemical potential difference between the empty hydrate and liquid water is calculated using

$$\begin{aligned}\frac{\Delta\mu_w^{\beta-L}}{T} &= \frac{\Delta\mu_L^{\beta-L}}{T_0} + \frac{P \cdot \Delta v^{\beta-L}}{T} + \left[\Delta h_0^{\beta-L} - \Delta C_p^{\beta-L} \cdot T_0\right]\left(\frac{1}{T} - \frac{1}{T_0}\right) - \\ &\quad \Delta C_p^{\beta-L} \cdot \ln\left(\frac{T}{T_0}\right) - R \cdot \ln\left(a_w\right)\end{aligned} \tag{3-32}$$

The chemical potential of water in the hydrate phase is then given by subtracting equations 3-29 and 3-32

Table 3-4: Physical constants for empty hydrate lattice in equilibrium with liquid water at 273.15 K, taken from [Munck et al., 1988].

$\Delta\mu_0^{\beta-L}$	1264	[J/mol]
$\Delta v^{\beta-L}$	$4.6 \cdot 10^{-6}$	[m^3/mol]
$\Delta h_0^{\beta-L}$	-4858	[J/mol]
$\Delta C_p^{\beta-L}$	39.16	[J/mol/K]
a_w	$\gamma_w \cdot x_w$	

$$\Delta\mu_w^H = \Delta\mu_w^{\beta-H} - \Delta\mu_w^{\beta-L}. \tag{3-33}$$

The fugacity of water in the hydrate phase is calculated by

$$f_w^H = f_w^\beta \cdot exp\left(\frac{-\Delta\mu_w^H}{R \cdot T}\right) \tag{3-34}$$

with

$$f_w^\beta = P_w^{sat,\beta} \cdot \phi_w^{sat,\beta} \cdot exp\left(\frac{V_w^\beta \left(P - P_w^{sat,\beta}\right)}{R \cdot T}\right). \tag{3-35}$$

The vapor pressure of the empty hydrate lattice $P^{sat,\beta}$ and the molar volume of the empty hydrate V_w^β are given by [Klauda and Sandler, 2000] as

$$P_w^{sat,\beta} = exp\left(4.1539 \cdot \ln(T) - \left(\frac{5500.9332}{T}\right) + 7.6537 - 16.1277 \cdot 10^{-3} \cdot T\right) \tag{3-36}$$

in which $P^{sat,\beta}$ is in [atm] and

$$\begin{aligned} V_w^\beta &= \left(11.835 + 2.217 \cdot 10^{-5} \cdot T + 2.242 \cdot 10^{-6} \cdot T^2\right) \frac{10^{-30} \cdot T \cdot N_a}{n_w} \\ &\quad -8.006 \cdot 10^{-9} \cdot P + 5.448 \cdot 10^{-12} \cdot P^2 \end{aligned} \tag{3-37}$$

with P in [MPa].

The relation for the calculation of the chemical potential and fugacity of water in the hydrate phase is described more extensively by [Sloan and Koh, 2008] and [Munck et al., 1988]. The fugacity coefficient of water in the hydrate phase is calculated by rearranging equation 3-26 to

$$\phi_i = \frac{f_i}{P \cdot x_i}. \tag{3-38}$$

Carbon dioxide

The fugacity of CO_2 in the hydrate phase is calculated from the simplified procedure of [Cole and Stephen P, 1990] proposed by [Michelsen, 1991].

$$f_{CO_2} = \frac{N_{CO_2}}{N_0} \cdot \frac{1}{C_{CO_2,l}} \cdot \frac{1}{\epsilon + \alpha_{CO_2} \cdot (1 - \epsilon)} \tag{3-39}$$

in which the amount of CO_2 per mole water

$$N_{CO_2} = \frac{x_{CO_2}}{x_w} \tag{3-40}$$

The number of empty lattices N_0 is defined as

$$N_0 = v_s + v_l - N_{CO_2} \tag{3-41}$$

and the ratio of the ratio of the Langmuir constants for CO_2 in the small and the large cavities

$$\alpha_{CO_2} = \frac{C_{CO_2,s}}{C_{CO_2,l}}. \tag{3-42}$$

The Langmuir constants $C_{CO_2,s}$ and$C_{CO_2,l}$ are defined by equation 3-31.

The ratio of free large lattice sites to the total free lattice sites ϵ is calculated by solving the function

$$F(\epsilon) = N_{CO_2} \cdot \frac{\epsilon}{\epsilon + \alpha_{CO_2} \cdot (1 - \epsilon)} + \epsilon \cdot N_0 - v_s = 0 \tag{3-43}$$

for ϵ.

The fugacity coefficient of CO_2 in the hydrate phase is calculated using equation 3-38.

3-2-3 Thermodynamic equilibrium

The thermodynamic equilibrium pressure and corresponding fugacity coefficients of the three phase system, has to meet three conditions:

1. Temperature equilibrium of all phases
2. Pressure equilibrium of all phases
3. Equality of chemical potential of a component in each phase

The equilibrium fugacities, a specific case of the thermodynamic model, are calculated for a given temperature by equaling the fugacity of the empty hydrate and the fugacity of liquid water. Naturally, as the fugacity of each component should be equal to each other in all phases, the fugacity of the vapor phase should be equal to that of the liquid and hydrate phase. This is used to validate the thermodynamic model, see section 3-5-1.

$$f_w^L = f_w^H \left(= f_w^V\right) \tag{3-44}$$

The calculated equilibrium pressure is used in the calculation of the fugacity coefficients in the hydrate-liquid phase region, as the pressure in the system under study does not change, see figure 3-1.

In figure 3-3 a flow chart of the thermodynamic model is given. With temperature and liquid mole fraction of the solution as an input, the liquid phase and the vapor phase fugacity coefficients are calculated using the UNIQUAC equation. The vapor phase fugacity is used to determine the fugacity of water in the hydrate phase. With the fugacity a new pressure is calculated and the algorithm is iterated until the difference between fugacity of water in the liquid phase and the vapor phase is smaller than the error of 10 Pa.

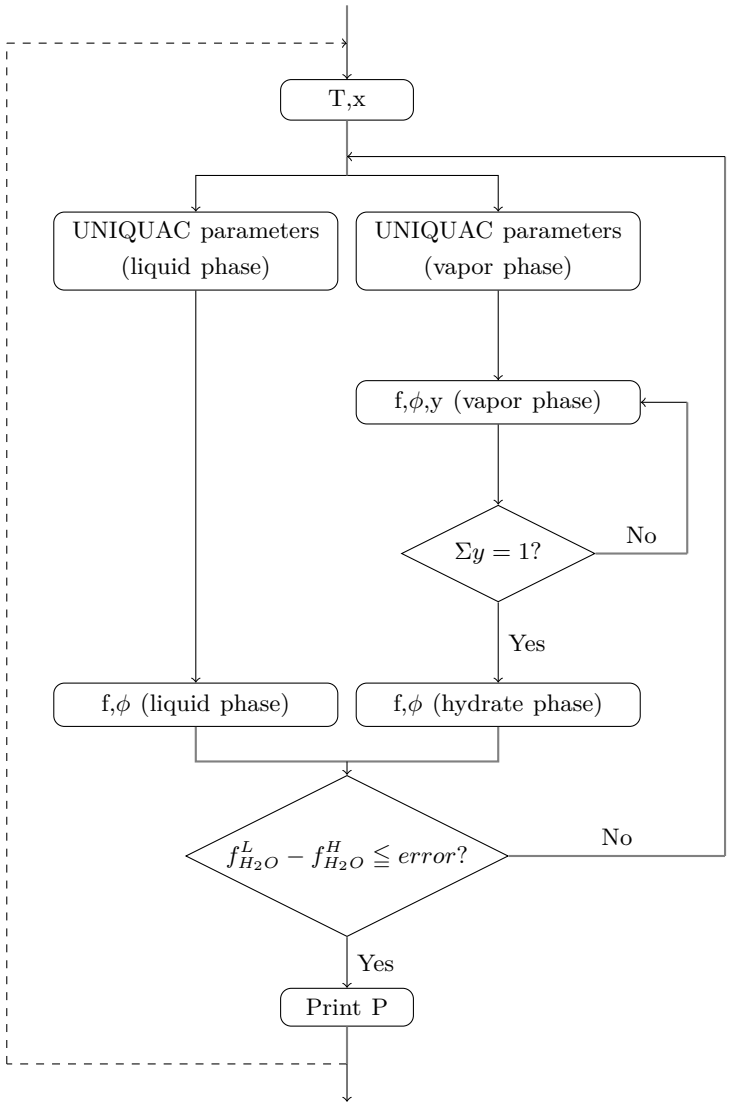

Figure 3-3: Flow chart of the thermodynamic equilibrium model with error = 10 Pa. For a given temperature (T) and liquid mole fraction (x), the UNIQUAC parameters are used to calculated the fugacities (f) and fugacity coefficients (ϕ) of the fluid phases (see section 3-2-1). The model proposed by [Van Der Waals and Platteeuw, 1959b] is used to determine the fugacity of water in the hydrate phase (section 3-2-2). The model iterates until the difference of the fugacity of water in the liquid phase and the hydrate phase is smaller than 10 Pa.

3-3 Flash calculation

"Flashing" is the partial evaporation of a liquid at a pressure equal or greater than its bubble point pressure when the pressure is reduced, producing a two phase system of vapor and liquid in equilibrium. The solution of the flash calculation is stable when a global minimum of the Gibbs energy is obtained. Flash calculation involves material balances and properties (fugacity coefficients, density) from a thermodynamic model [Ness et al., 2005].

For the three phase (liquid, vapor and solid) flash calculation, a method proposed by [Gupta et al., 1991], applicable to both reacting and non-reacting systems, is used, which includes a stability analysis algorithm to ensure a global minimum of the Gibbs energy is obtained and not a local minimum.

Iterating for mole fractions in a phase, rather than the mole numbers, has the advantage that those mole fractions are always defined, even if its phase fraction becomes zero. The model algorithm computes simultaneously the stability and multiphase equilibria of a system, using the Newton-Raphson method, a method to numerically solve algebraic equations. This is required since the number of phases present is unknown a priori.

The first condition for solving the algorithm is the summation of the phase fraction, which should be equal to 1:

$$\sum_{k=1}^{\pi} \beta_k = 1. \tag{3-45}$$

The mole fractions are summed as

$$\sum_{i=1}^{N} \left(K_{ik} \cdot exp\left(\Omega_k\right) - 1\right) \cdot x_{ir} = 0 \qquad (k = 1, ..., \pi;\ k \neq r) \tag{3-46}$$

with

$$x_{ir} = \frac{n_i}{n_t \cdot D_i} \qquad (i = 1, ..., N) \tag{3-47}$$

where the total amount of moles in the system is

$$n_t = \sum_{i=1}^{N} n_i \tag{3-48}$$

and

$$D_i = 1 + \sum_{j=1}^{\pi} \left(K_{ij} \cdot exp\left(\Omega_j\right) - 1\right) \cdot \beta_j \qquad (j \neq r)\,. \tag{3-49}$$

N is the number of components and π the number of phases. The distribution coefficient K_{ik} of component i in phase k is defined as the ratio of the corresponding fugacity coefficients and is by definition also equal to the mole fraction ratio:

$$K_{ik} = \frac{\phi_{ir}}{\phi_{ik}} = \frac{x_{ik}}{x_{ir}}. \tag{3-50}$$

Equation 3-50 is valid only for phases present at thermodynamic equilibrium, so it can be used only if all phases are present. The phases present at equilibrium are not known a priori for hydrate forming mixtures and [Gupta et al., 1991] solved this by defining the mole fractions as

$$x_{ik} = K_{ik} \cdot x_{ir} \cdot e^{\Omega_k} \qquad (i = 1, ..., \pi;\ k \neq r)\,, \tag{3-51}$$

If phase β_k is present, the stability variable $\Omega_k = 0$. At the final solution, which is when the Gibbs free energy is at a minimum, the stability variable Ω_k satisfies

$$\Omega_k = \ln\left(\frac{f_{ik}}{f_{ir}}\right). \tag{3-52}$$

Using the constraints

$$\beta_k \cdot \Omega_k = 0 \qquad (k = 1, ..., \pi;\ k \neq r)\,. \tag{3-53}$$

and

$$\beta_k \geqq 0 \qquad and \qquad \Omega_k \geqq 0 \tag{3-54}$$

the mole fractions and phases can be calculated. The constraint in equation 3-54 means that either the phase fraction β_k or the stability variable Ω_k, or both, must be zero. A flow chart of the flash model is given in figure 3-4.

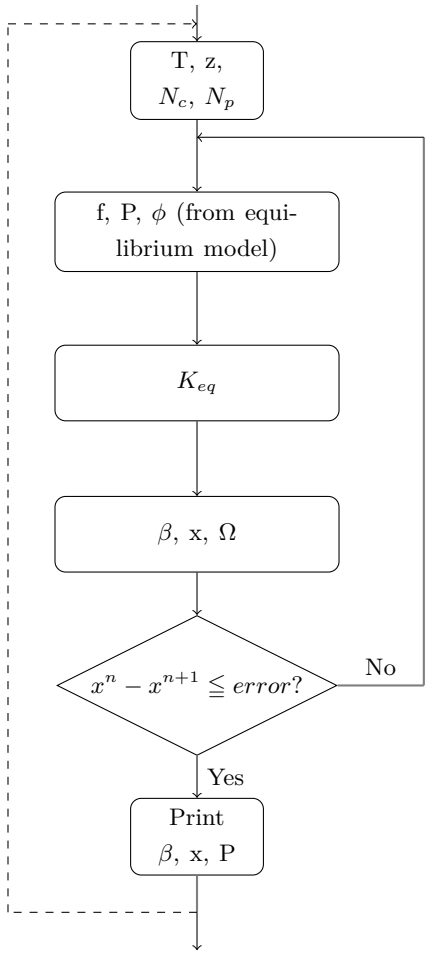

Figure 3-4: Flow chart of the flash model, taking into account hydrate formation. The temperature (T), overall mole fraction (z), number of components (N_c) and number of phases (N_p) are used to determine the equilibrium constant (K) with fugacity coefficients from the thermodynamic model (see section 3-2. With that, the phase fractions (β), the mole fractions of the components in each phase (x) and the stability variable (Ω) are iterated until the difference between the calculated mole fractions in two subsequent iterations are smaller than 10^{-4}.

3-4 Density calculation

With the growth model implemented, the mass fraction of the hydrates in the mixture can be calculated from the amount of moles of hydrate that are formed. This is known from the amount of CO_2 consumed in the hydrate phase, see equation 3-3, and the mole fraction of H_2O per hydrate, known from the thermodynamic model.

The specific volume of the hydrate slurry can be written as

$$V_{slurry} = V_{sol} \cdot w_{sol} + V_H \cdot w_H \tag{3-55}$$

with the mass fraction $w_{sol} = (1 - w_H)$ and $V = \frac{1}{\rho}$. Rearranging equation 3-55 gives an expression for the density of the hydrate slurry.

$$\rho_{slurry} = \frac{\rho_{sol} \cdot \rho_H}{\rho_{sol} \cdot w_H + \rho_H \cdot (1 - w_H)}. \tag{3-56}$$

The density of the CO_2 hydrate can be calculated by a relation proposed by [Teng et al., 1996]

$$\rho_H = \frac{46 \cdot M_{CO_2}}{N_a \cdot s^3} \left(0.409 + \frac{x^H_{CO_2}}{1 - x^H_{CO_2}} \right) \tag{3-57}$$

with the lattice dimension s (see table 2-1) in meters, which is 12 Å $(12 \cdot 10^{-10}\, m)$ for CO_2, and N_a the Avogadro constant. The relation between the cavity occupancy θ and the molar fraction of CO_2 in the hydrate, $x^H_{CO_2}$, can be written as

$$\theta = \frac{5.75 \cdot x^H_{CO_2}}{1 - x^H_{CO_2}} = \frac{8}{x + y} \tag{3-58}$$

in which $x \leqslant 2$ and $y \leqslant 6$, referring to the small and large cavities in structure I hydrates, see table 2-1. The cavity occupation is variable as hydrates are non-stoichiometric compounds, and so the density of the hydrates depends on the cavity occupation, varying between 1134 and 1049 kg/m^3 [Hu et al.].

[Duan et al., 2008] reports the existing models for equilibrium conditions to be insufficiently accurate for the prediction of density and other volumetric properties and proposes a model for the calculation of the specific volume of a $H_2O - CO_2$ solution V_{sol} as

$$V_{sol} = V_{H_2O} \left[1 + (A_1 + A_2 \cdot P) \cdot x_{CO_2} \right] \tag{3-59}$$

with

$$A_i = A_{i1} \cdot T^2 + A_{i2} \cdot T + A_{i3} + A_{i4} \cdot T^{-1} + A_{i5} \cdot T^{-2} \tag{3-60}$$

where the constants A_{ij} are given in table 3-5. The mole fraction CO_2, x_{CO_2}, dissolved in water is known from the flash model.

Table 3-5: Constants A_{ij} for calculation of the specific volume of the $H_2O - CO_2$ mixture in equation 3-60.

j	A_{1j}	A_{2j}
1	$0.38384020 \cdot 10^{-3}$	$-0.57709332 \cdot 10^{-5}$
2	$-0.55953850 \cdot 10^{0}$	$0.82764653 \cdot 10^{-2}$
3	$0.30429268 \cdot 10^{3}$	$-0.43813556 \cdot 10^{1}$
4	$-0.722044305 \cdot 10^{5}$	$0.10144907 \cdot 10^{4}$
5	$0.63003388 \cdot 10^{7}$	$-0.86777045 \cdot 10^{5}$

The density of the $H_2O - CO_2$ solution can be calculated from

$$\rho_{sol} = \frac{1}{V_{sol}}. \tag{3-61}$$

The predicted solution density from the model is compared with the measured density from the experimental set-up in section 4-4.

3-5 Model validation

To validate the developed models, they are compared with data from literature. Some results are qualitatively validated if no experimental data are available. The thermodynamic model and the flash model are validated separately in sections 3-5-1 and 3-5-2.

3-5-1 Thermodynamic model

The thermodynamic model is validated by simulating the equilibrium conditions and comparing them with experimental data. Equilibrium pressures for H_2O-CO_2 systems are available from literature, an extensive list of equilibrium data for several hydrate forming gases, including CO_2, is made available in [Sloan and Koh, 2008]. A selection of this data is used for comparison with the developed model, see figure 3-5.

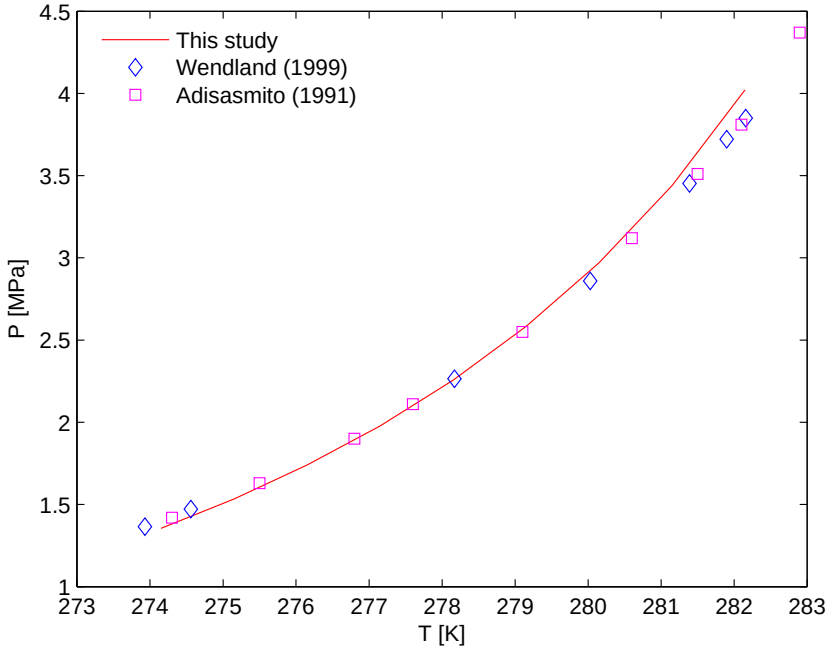

Figure 3-5: Predicted equilibrium pressure compared with experimental data from [Wendland et al., 1999] and [Adisasmito et al., 1991].

Figure 3-5 shows that the deviation from experimental data found in literature increases with increasing temperature. The model appears to predict a higher value of the equilibrium pressure. The highest temperatures on the equilibrium line are however not of interest for this study.

The relative error of the predicted equilibrium pressure with the data from [Wendland et al., 1999] is between 0.15 and 4.42% and with the data from [Adisasmito et al., 1991] between 0.51 and 4.48 %. In both comparisons, the largest deviations occur at the higher temperatures (280.6 - 282.9 K).

The maximum relative deviation (see equation 3-62), average absolute deviation (see equation 3-63) and the maximum absolute deviation are given in table 3-6.

The relative deviation is defined as

$$RD = 100 \cdot \frac{|P_{exp,i} - P_{mod,i}|}{P_{exp,i}} \tag{3-62}$$

and the average absolute deviation as

$$AAD = \frac{1}{N} \cdot \sum_{i=1}^{N} |P_{exp,i} - P_{mod,i}|. \tag{3-63}$$

Table 3-6: Absolute average deviation (AAD), maximum absolute deviation (AD_{max}) and maximum relative deviation (RD_{max}) between the predicted equilibrium pressure and the experimental equilibrium pressure from [Wendland et al., 1999] and Adisasmito1991.

	AAD [MPa]	AD_{max} [MPa] (at T [K])	RD_{max} [%] (at T [K])
[Wendland et al., 1999]	0.084	0.18 (282.16)	4.42 (282.16)
[Adisasmito et al., 1991]	0.073	0.20 (282.90)	4.48 (282.10)

At equilibrium conditions, the fugacities of a component in all (three) phases are equal as can be seen in figure 3-6.

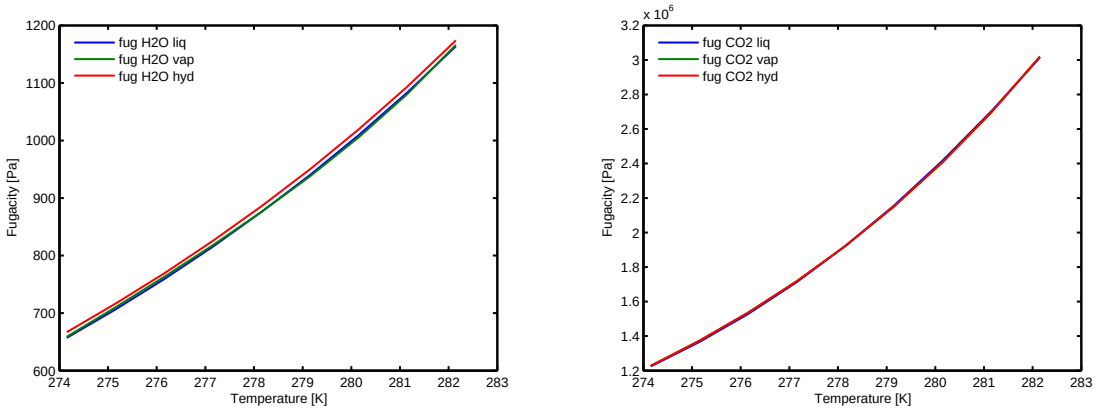

(a) H_2O (b) CO_2

Figure 3-6: Fugacities of the vapor, liquid and hydrate phase of H_2O in figure 3-6(a) and CO_2 in 3-6(b) at equilibrium conditions.

3-5-2 Flash model

The calculated mole fraction of CO_2 in the liquid phase is compared with the known solubility of CO_2 in water [Diamond and Akinfiev, 2003], at equilibrium conditions. Good agreement is observed between the predicted values and the values from [Diamond and Akinfiev, 2003], see figure 3-7(a).

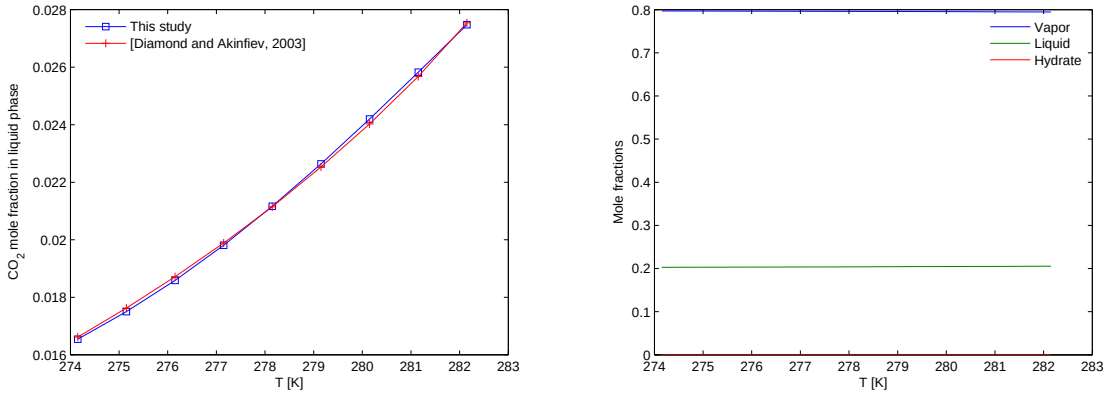

(a) CO_2 mole fraction in the liquid phase.

(b) Mole fractions of the three phases.

Figure 3-7: Validation of flash model at equilibrium conditions with in figure 3-7(a) the CO_2 liquid phase mole fraction from the developed model and the model from [Diamond and Akinfiev, 2003] and in figure 3-7(b) the mole fraction of the three phases (vapor, liquid and hydrate).

Furthermore, at equilibrium conditions, no hydrates should be formed, thus its phase fractions should be zero. The fractions of the liquid and vapor phase are approximately equal to their initial values (0.2 for the liquid phase, 0.8 for the vapor phase), see figure 3-7(b).

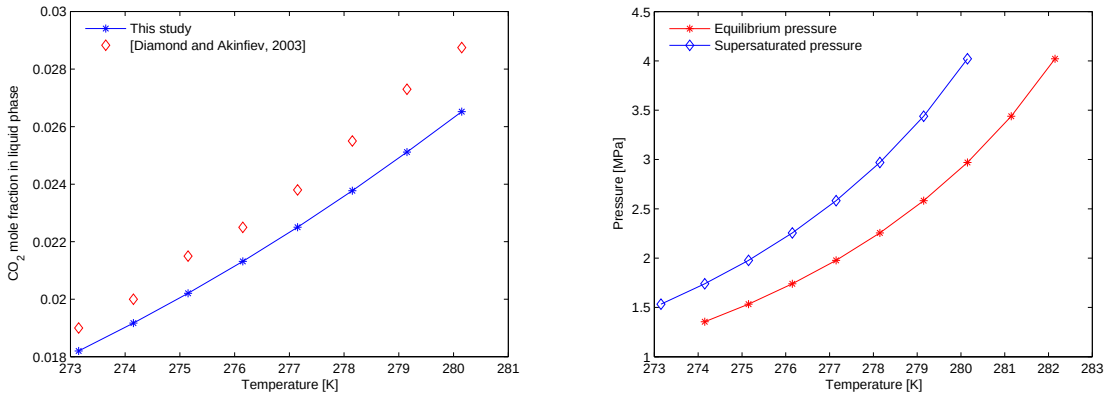

(a) CO_2 liquid phase mole fractions.

(b) Pressure.

Figure 3-8: The predicted liquid phase CO_2 mole fraction in supersaturated conditions are compared with data from [Diamond and Akinfiev, 2003] in figure 3-8(a) at a driving force of 2 K, which corresponds to the pressure-temperature line in figure 3-8(b).

In the liquid-hydrate region however, the mole fractions deviate. In figure 3-8(a) the CO_2

mole fraction in the liquid phase is presented and compared with data from [Diamond and Akinfiev, 2003], at a driving force of 2 K. At these conditions (see figure 3-8(b)) the relative error is between 4.2 and 8.0 %.

This might be caused by the calculation of the fugacity components in the thermodynamic model. The H_2O hydrate fugacity in that model is calculated with the cavity occupancy (see equation 3-30), using the fugacity of CO_2 in the vapor phase. This is also done by [Sabil, 2009] and [Hartono, 2011]. The model does not converge when the fugacity of CO_2 in the hydrate phase (see equation 3-39) is used. At equilibrium conditions, when the fugacities of a component are equal in all phases, this does not cause deviations in the predicted fugacities, but in the hydrate-liquid region an incorrect fugacity coefficient results in incorrect mole fractions from the flash calculation.

The deviation of the model increases slightly with increasing temperature. This might be caused by the deviations in the predicted equilibrium pressure, which also increase with temperature, see figure 3-5-1.

3-6 Discussion

The thermodynamic model, validated at equilibrium conditions, is able to predict the pressure and fugacities of the $H_2O - CO_2$ system. The binary energy parameters, u_{ij}, are determined by fitting the H_2O fugacity in the vapor phase to that of the liquid and hydrate phase. The $H_2O - CO_2$ interaction has a big influence on that value, in contradiction to the $CO_2 - H_2O$ interaction. That one however seems to have an influence on the fugacity of CO_2, which may cause deviations in the calculated mole fractions in the flash model. A more thorough investigation on this interaction parameters might be useful when the modeling deviations are to be minimized.

The flash model, does not predict the mole fractions in the hydrate region accurately, which might be caused by incorrect fugacity coefficients from the thermodynamic model. The fugacity of H_2O in the hydrate phase is calculated with the cavity occupancy, which uses the vapor phase fugacity of CO_2. The flash model does not converge when the fugacity of CO_2 in the hydrate phase, as described in section 3-2-2, is used.

At equilibrium conditions however, as the fugacities in all phases are equal, the flash model predicts the mole fractions correct. These are presented in figure 3-9.

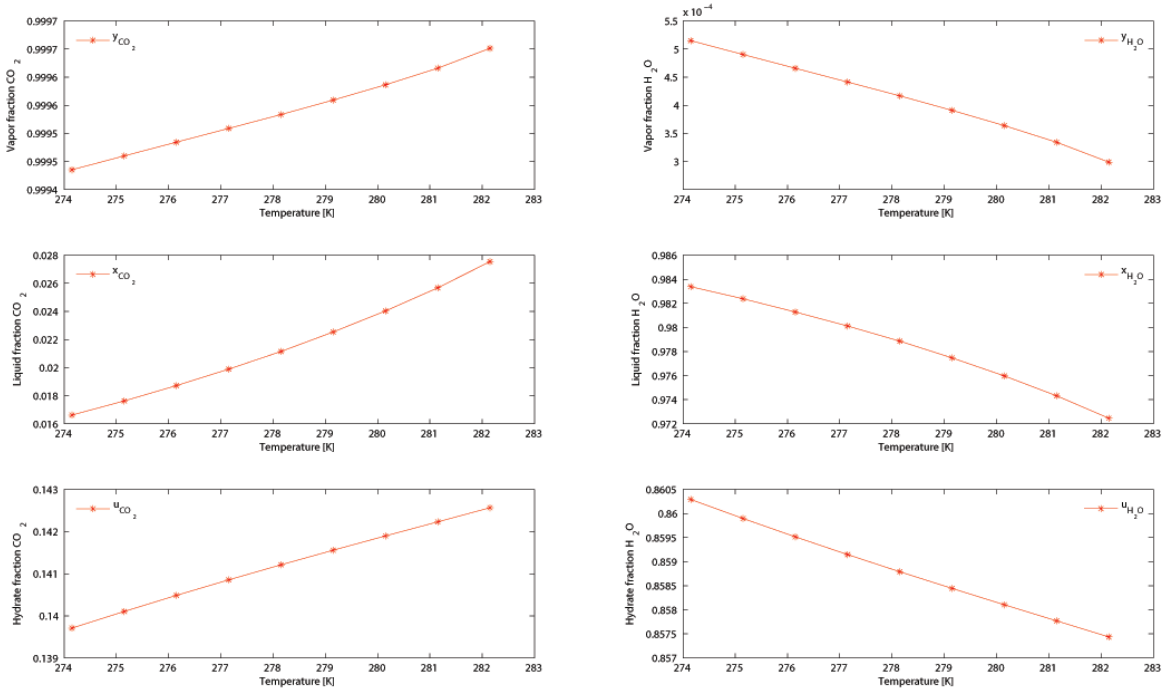

Figure 3-9: Resulting mole fractions from the flash calculation at equilibrium conditions. On the top row the vapor phase (y), the middle row the liquid phase (x) and the bottom row the hydrate phase (u). The left column are the CO_2 mole fractions, the right column H_2O mole fractions.

The model does predict the hydrate phase to be present at supersaturated conditions, see figure 3-10. As induction or growth are not accounted for in the flash model, the occurrence of hydrates is instantaneous in the flash model.

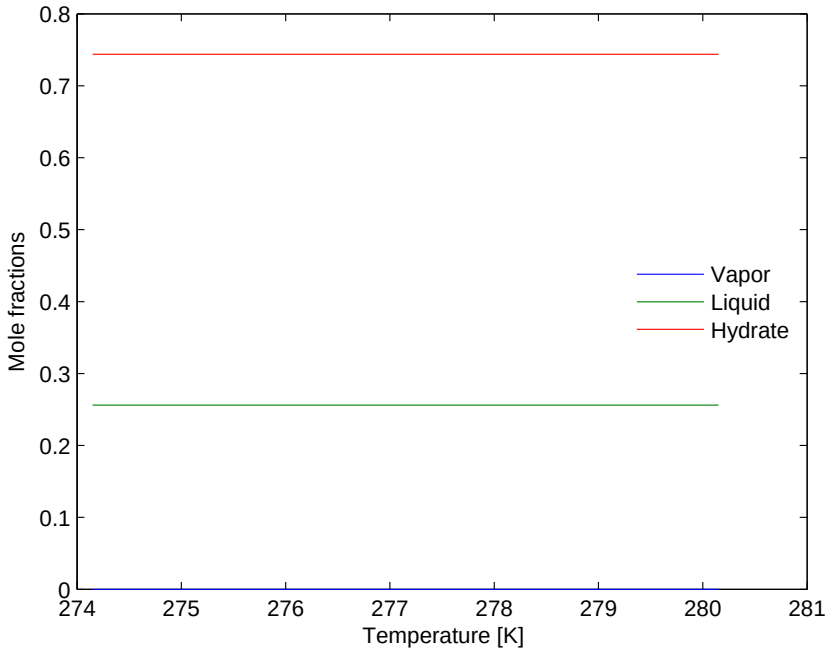

Figure 3-10: Mole fractions of the phases present at supersaturated conditions (2K).

Chapter 4

Experiments

A system is designed for continuous CO_2 hydrate production and constructed during this study. Hydrates are produced and measurements performed on the slurry density. A sample can be taken from the produced hydrate slurry, which can be used later to cool meat and investigate the influence on the meat in a specialized laboratory. An indication of the amount of hydrates required to cool a certain mass of meat is given in appendix A. The system and its components are described in section 4-1. The experimental methodology and operating instructions are given in section 4-2 and the results of the experiments are presented in section 4-3.

4-1 Experimental set-up

The developed system consists of two thermostatic baths, a pump, two vessels, two coil heat exchangers and auxiliary instrumentation and equipment. The details and selection of suitable components, like the pump and sight glasses, and the instrumentation are done in close collaboration with IBK Groep, who constructed the set-up. After performing first experiments and improving some details of the configuration, the set-up is relocated to the Process & Energy department at Delft University of Technology. More experiments are performed here and will be performed in the future. In the future the set-up will also be moved to Lunenburg Vlees B.V. in Oudewater to perform experiments on meat with the produced hydrates in their laboratory.

Figure 4-1: Photograph of the developed experimental CO_2 hydrate production set-up.

4-1-1 Process description

The hydrate formation process in the designed system can be described by a number of subsequent steps. The numbers in the process flow and instrumentation diagram (see figure 4-2) correspond with the numbers of the process description in this section.

1. The system is filled with water and pressurized with CO_2.
2. The mixture is cooled down to hydrate formation conditions in thermostatic bath 1 and 2.
3. The hydrate slurry is separated from the excess CO_2 gas in one of the two vessels.
4. The hydrate slurry is either pumped to thermostatic bath 2 (4a) or a sample is taken (4b) or (4c).
5. If necessary, the hydrates are dissociated in thermostatic bath 2.

For the hydrate formation the H_2O-CO_2 mixture will be cooled to a temperature between 276 to 284 Kelvin at pressures between 10 and 40 bar, depending on the process conditions at which the hydrates will be produced. The hydrates can be dissociated by heating the slurry or by decreasing the pressure.

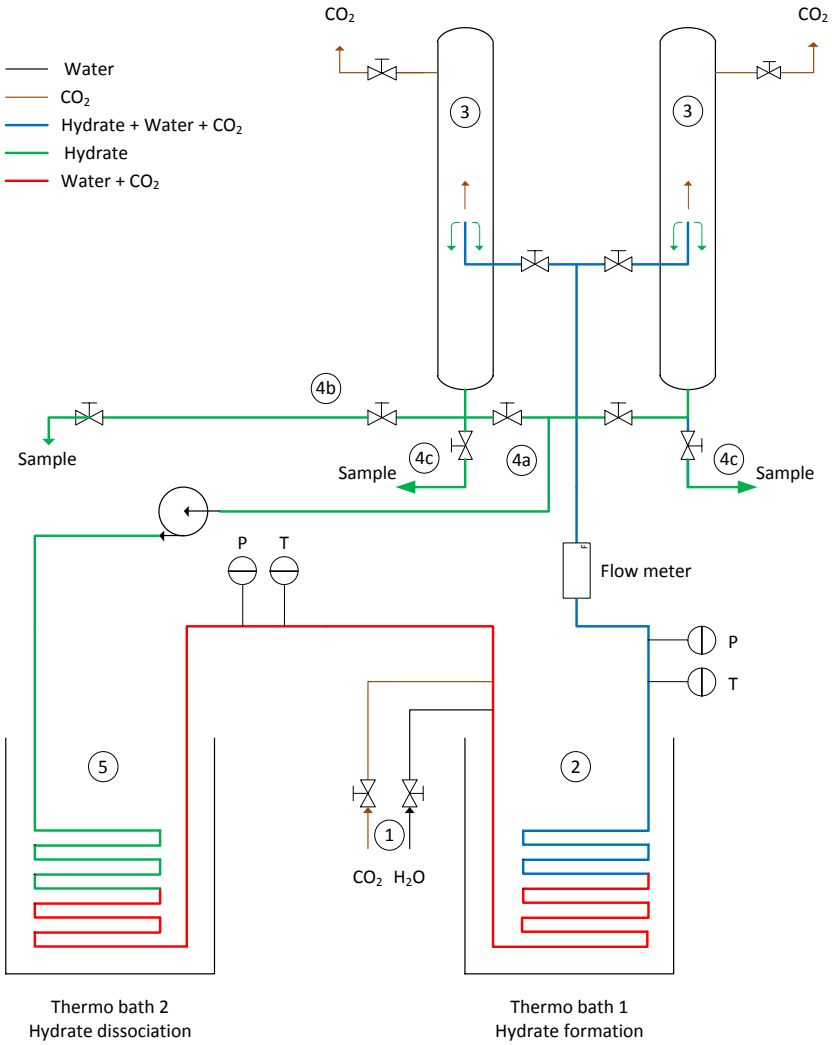

Figure 4-2: Schematic representation of the hydrate production set-up.

4-1-2 System components

Pump

The flow is circulated with a Gather gear pump (0.37 kW), with a maximum flow of 100 dm^3/hr. The pump speed is adjustable by setting the frequency manually with a potentiometer.

Thermostatic baths

The hydrates are formed and dissociated in two Lauda RC 20 thermostatic baths, which can operate at temperatures controlled by a PID controller between -35 and 150 °C. The dimension of the filling volume are 300 mm x 175 mm x 140 mm (width x depth x height), giving a maximum filling volume of 10 to 14 dm^3.

The baths have a maximum heating power of 2 kW and an effective cooling capacity of 0.3 kW with ethanol when the bath temperature is 20 °C and the ambient temperature 20 °C.

The thermostatic baths are either filled with water when the bath temperature will remain above 5 °C or with a water-ethanol mixture with freezing point around -5 °C for lower bath temperatures. The temperature of the baths are measured by a built in temperature probe with an absolute accuracy of 0.2% of reading ±0.2 K.

Tubes

Stainless steel tubes are used with an inner diameter of 6 mm at the pressure side and 8 mm at the suction side of the pump. A flow of 100 dm^3/hr will result in a flow speed of about 1 m/s. A stainless steel tube with a inner diameter of 2.5 cm and a length of 1 meter is connected to the outlet of the vessels, an can be closed off on both sides. With this tube a sample of the hydrate slurry can be taken.

Sight glasses

Four sight glasses in stainless steel housings are installed, one in each vessel to visually inspect the level of hydrates in the vessels and two in the hydrate flow, one before and one after the thermostatic bath in which the hydrates are formed. Maximum operating pressure of the glasses is 40 bar.

Vessels

The two identical vessels have a volume of 3 dm^3 and are equipped with a pressure safety valve. The hydrate flow is injected at the same height as the sight glasses and both vessels can be shut off from the slurry loop, allowing sampling of hydrates from one of the vessels. The vessels are designed for a maximum operating pressure of 40 bar and equipped with corresponding safety relief valves.

Hydrate sample

A hydrate sample can be taken by filling a fixed volume with hydrates by opening a valve a the entrance of a 1 meter long tube with an inner diameter d_i of 2.5 cm. When the tube is filled and the valve closed, another valve at the outlet of the tube is opened to take out the hydrate sample.

With this a volume of

$$V_{sample} = \pi \cdot \left(\frac{d_i}{2}\right)^2 \cdot L = \pi \cdot \left(\frac{2.5 \cdot 10^{-2}}{2}\right)^2 \cdot 1 = 4.9 \cdot 10^{-4}\, m^3 \tag{4-1}$$

is taken and can be used to cool a sample of meat.

Figure 4-3: Photograph of a hydrate sample.

Drawback of taking a sample from this fixed volume is the pressure drop when the hydrates are stored in the sample volume for short period. Furthermore, the temperature of the stainless steel sample volume is higher than the the temperature of the mixture, and dissociation might occur.

Another way of taking a sample is by directly purging it from the suction line of the pump. By running the water-hydrate mixture through a sieve which is placed on a balance, the mass of the sample can be determined. With this method, the crystal size can be estimated by using different mesh sizes for the sieve. The crystal size during the conducted experiments is determined to be between 90 and 150 micrometer.

4-1-3 Instrumentation

A data acquisition system from ATAL collects the data from the pressure and temperature sensors in the flow, the temperature of both thermostatic baths and the density measurement from the flow meter. The data can be read real time during the experiments and exported to '.xls' format for data analysis in MS Excel.

Pressure transmitter

The system pressure is measured before and after the hydrate formation in thermo bath 1. Siemens SITRANS P DS III 7MF4033-1EA00-1AB1 pressure transmitters are used, which are applicable in a range from 0.63 to 63 bar with the measurement error listed in table 4-1. The total measurement error can be calculated by the least square method (square root of the sum of the individual errors squared), for a set span of 40 bar the absolute measurement error is 0.097 bar.

Table 4-1: Measurement errors for the Siemens pressure transmitter.

	Measurement error	Relative error
Linear error (r $\leqslant$10)[a]	$\leqslant (0.0029 \cdot r + 0.071)\%$ [a]	0.076%
Long-term drift (temp. change $\pm$30°C)[b]	$\leqslant (0.125 \cdot r)\%$ per 5 years [a]	0.039%
Influence of ambient temp. (-10...+60 °C)	$\leqslant (0.08 \cdot r + 0.1)\ \%$ [a]	0.226%
Total error (least square method)		0.242%

[a] $r = \frac{Max.\ span}{Set\ span} = \frac{63}{40} = 1.575$

[b] Long-term drift error can be divided by 5 for small operational times

Temperature sensor

The temperature of the flow is measured before and after the hydrate formation in thermo bath 1. PT100 $\frac{1}{10}$DIN B sensors are used with an accuracy of $\pm(0.03 + 0.0005 \cdot T[°C])$, which results in an error of $\pm$0.03 K at 5 °C.

Flow meter

The flow is measured between the two thermo baths with a Proline Promass 80A flow meter from Endress+Hauser, which uses the Coriolis measurement principle to determine the physical fluid properties. The flow meter is used to measure the density, the measurement error for the liquid density is given by the supplier to be $\pm\, 0.02\, kg/dm^3$ over the entire measurement range of the sensor. This error decreases to $\pm\, 0.0005\, kg/dm^3$ at reference conditions (20 to 30 $°C$ and 2 to 4 bar for water).

4-1-4 Process conditions

The process conditions at which the experiments will be conducted are determined by the pressure and temperature of the hydrate forming mixture, see figure 4-4 and 2-1.

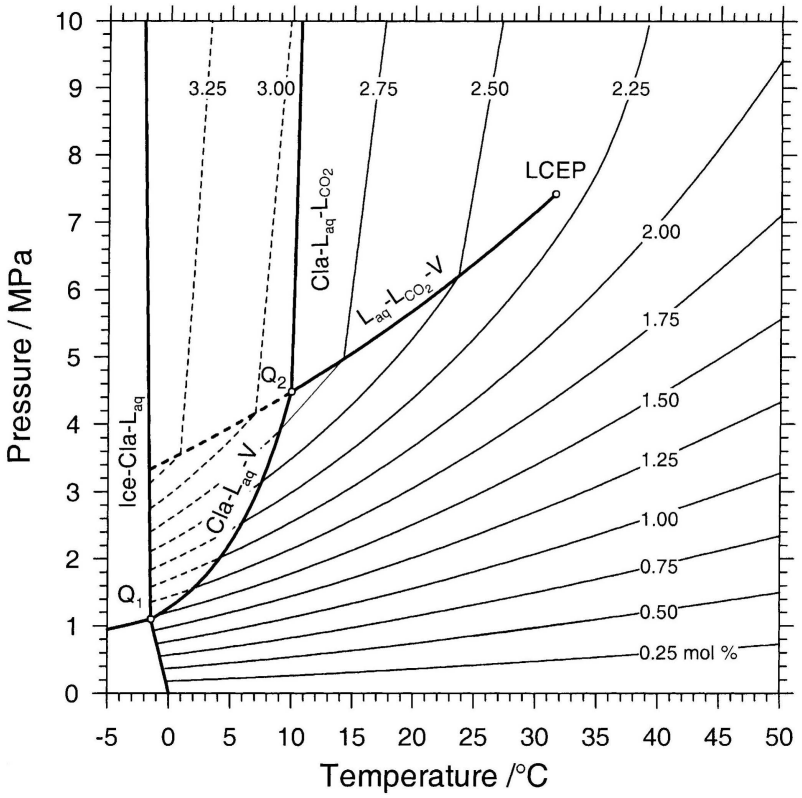

Figure 4-4: Phase diagram of the $H_2O - CO_2$ system with the CO_2 solubility isopleths. Taken from [Diamond and Akinfiev, 2003].

Pressure

The system pressure is set between 12 and 35 bar, depending on the temperature at which the hydrates are required. The set pressure is expected to decrease during cooling due to the increasing solubility of CO_2 in the liquid phase and the gas contraction that takes place.

Temperature

The hydrate forming mixture is cooled until hydrates are visible in the sight glasses. This will be at a lower temperature than the equilibrium temperature, as the formation process requires a supersatured state.

4-2 Experimental methodology

The numbers referring to system components in this section correspond with the indicators in the process flow & instrumentation diagram in figure 4-5.

1. The system is filled with demi-water, until both vessels are filled for approximately 50% with water. This is determined visually through the sight glasses in the vessels. Through these sight glasses the entrance tube is visible. Filling the vessel to a level higher than the flow entrances will result in better mixing of hydrates in the vessels once these are formed. Filling it to a lower level will cause the hydrates to agglomerate on the water surface. The pump is started during the filling of the system, this will distribute the water through the system.

2. The system is pressurized by adding CO_2 up to 30 bar, corresponding to an equilibrium temperature of 7 $°C$. The flow is set to 85 kg/hr by setting the frequency regulator to 27.50 Hz. Above a frequency of 27.50 Hz the mass flow measurement by the flow meter gives an error.

3. The thermostatic baths are set on a temperature equal to the equilibrium temperature corresponding to the system pressure. The temperature of the flow is about 2 K above the baths temperature.

4. Once the temperatures are stable, which is determined from the real time collected measurements from the data acquisition system, the system is cooled in steps of 0.5 K per 10 minutes. During cooling the temperature of thermostatic bath "Lauda 1" is set 0.5 K higher than the temperature of bath "Lauda 2", to ensure hydrate formation takes place in the colder "Lauda 2". This makes it possible to detect plugging of the heat exchangers, which results in a pressure difference op 8 bar between the inlet and the outlet of the heat exchangers, measured by pressure transmitters PT11.04 and PT11.06. At this pressure difference the pump starts to circulate the flow through the bypass.

5. As soon as hydrates are visible in the sight glass after the thermostatic bath in which the hydrates are formed (SG11.06), or the sight glasses of the vessels (SG11.09 and SG11.16), the temperature of both thermostatic baths is increased by 1 K to decrease the supersaturation of the system. The presence of the formed nuclei will ensure growth and/or formation of new nuclei.

6. When the hydrates are also visible in the sight glass on the suction side of the pump (SG11.21), the hydrates are mixed through the vessel. At this point one of the vessels is isolated from the circulating flow by closing valves V11.07 and V11.13 (or V11.14 and V11.20) to prevent a pressure drop in the whole system and a sample is taken. The slurry is sprayed through a hose connected to a tube that can be opened by valve V11.25 (or V11.24, depending on which vessel is isolated) on a sieve, placed on a balance. The hydrates collect on the sieve and the liquid water in a bucket under the sieve.

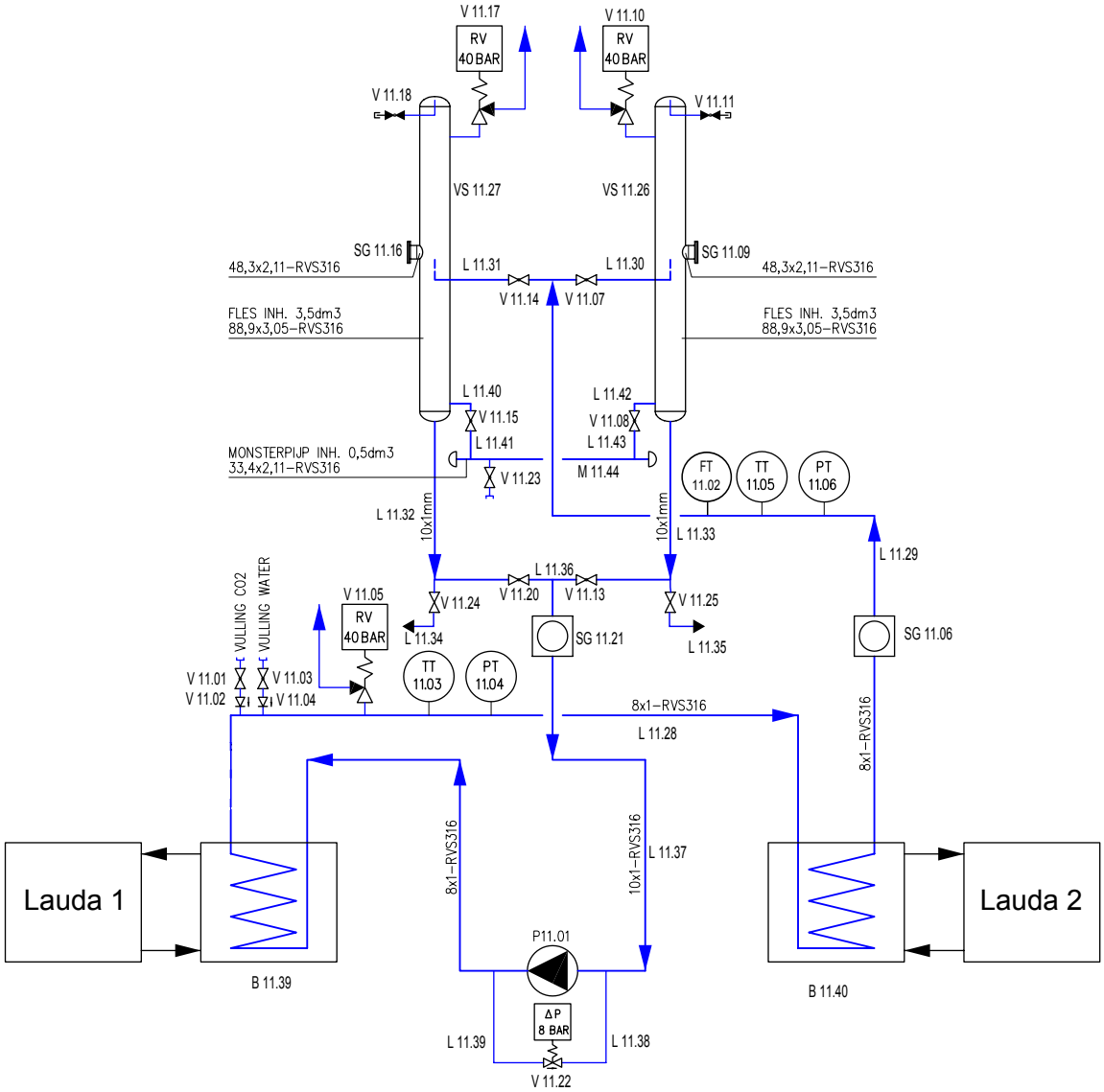

Figure 4-5: Process flow & instrumentation diagram of the hydrate production set-up.

Table 4-2: Indicators from the process flow & instrumentation diagram (figure 4-5).

Indicator	Meaning	Indicator	Meaning
B	Bath	RV	Relieve valve
FT	Flow transmitter	SG	Sigth glass
L	Tube	TT	Temperature transmitter
M	Sample volume	V	Valve
P	Pump	VS	Vessel
PT	Temperature transmitter		

4-3 Experimental results

The variation of the temperature and pressure during an experiment is presented in figure 4-6. The temperature difference between the thermostatic baths and the $H_2O - CO_2$ solution is about 2 K and will depend on the mass flow and the heat transfer fluid in the thermostatic bath (which is in the present study a 80/20 wt% water-ethylene glycol mixture). During the experiments the flow rate is always set on 85 kg/hr. In the experiment of figure 4-6 the pressure difference of 8 bar between the inlet and the outlet of the heat exchanger in thermostatic bath "Lauda 2" is visible at the end of the experiment, indicating the heat exchanger is plugged.

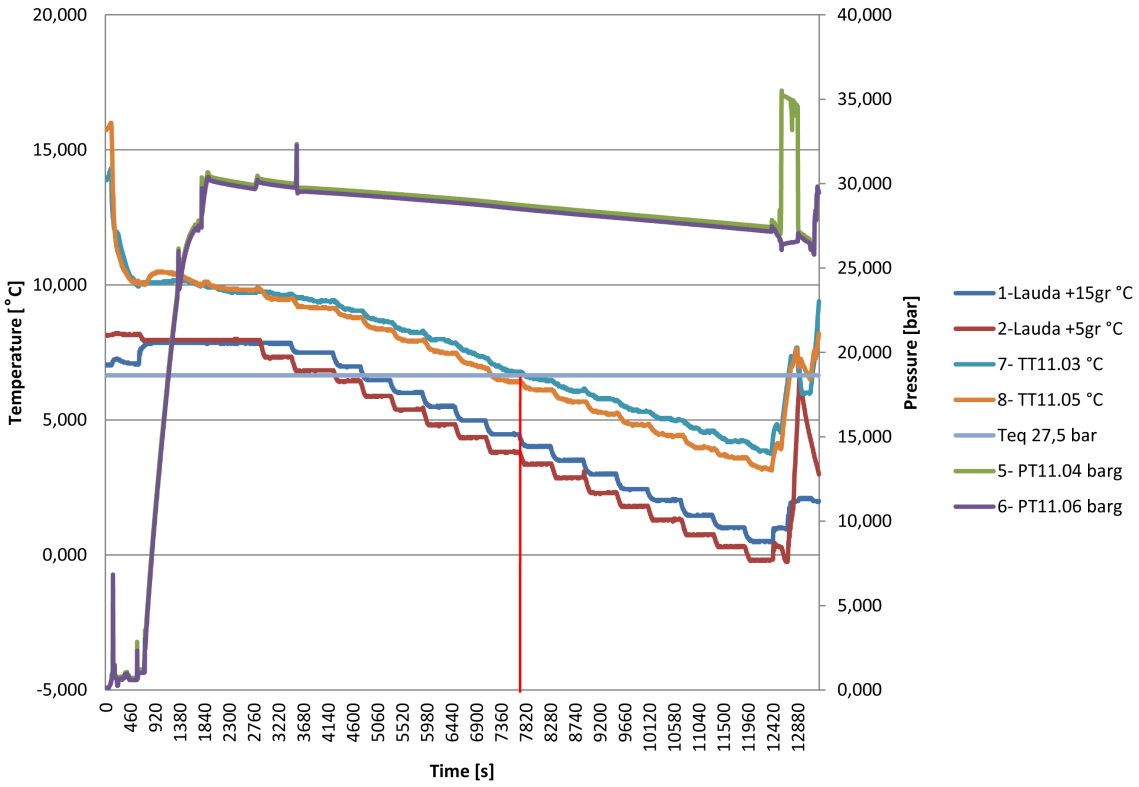

Figure 4-6: Sample of measured temperatures and pressures from an experiment. The vertical red line indicates from which point the $H_2O - CO_2$ mixture is supersaturated. The peak in the pressure before the hydrate forming bath (PT11.04) at the end of the experiment indicates that the heat exchanger is plugged.

In figure 4-7 the measured density from the experiment of figure 4-6 is presented. Until 1720 seconds from the start of the experiment, the density is equal to that of water (1000 kg/m^3). From that point CO_2 is added to the system, and fluctuations in the density are observed, as a lot of bubbles are present in the flow. This is visible as the concentration of peaks between 1720 and 2150 seconds after the start of the experiment. After that the density increases to just under 1014 kg/m^3, and increases further when more CO_2 is dissolved in the liquid water due to the decreasing temperature during the experiment.

A small peak can be observed at 12040 seconds from the start of the experiment, but the

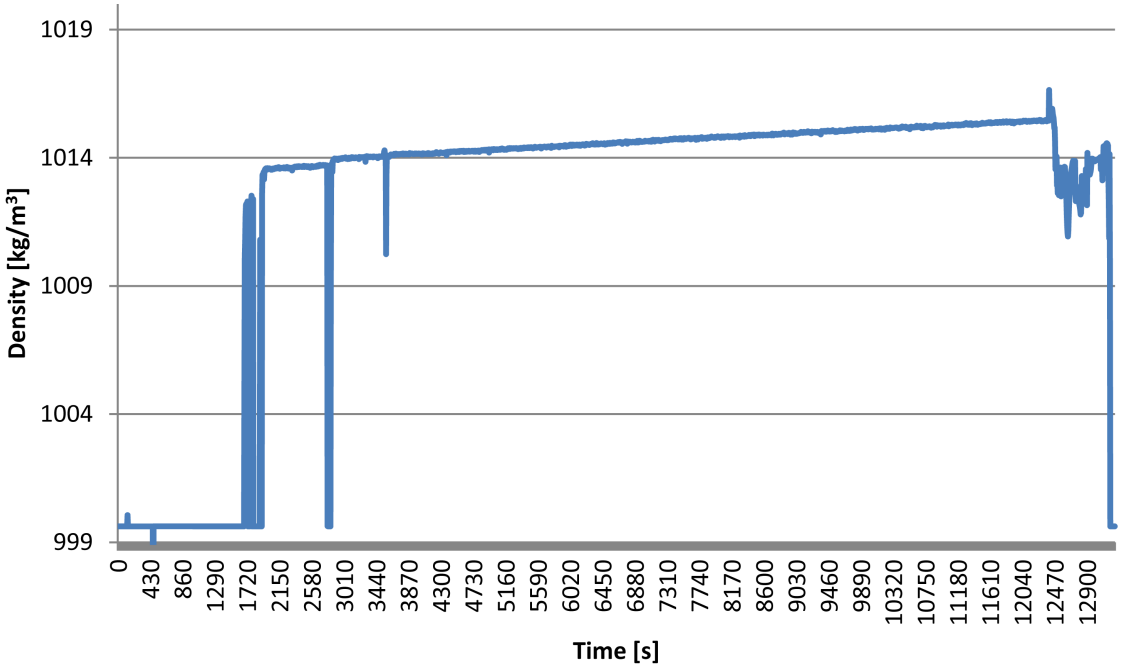

Figure 4-7: Measured density of the flow from the same experiment as shown in figure 4-6.

density does not show a constant increased value. This is in contradiction to what is shown by [Hu et al., 2010], reporting a density of 1022 kg/m^3 for a hydrate mass fraction of 38%. The peak is visible just before the plugging of the heat exchanger (see figure 4-6) and after that, the temperature is increased to dissolve the hydrates in this plugged heat exchanger. The lower density after the peak, can be explained by the increased temperature, as less CO_2 can be dissolved into water at a higher temperature.

The temperature at which hydrates form varied during different experiments. Hydrates appear to form easier when a trigger, like adding or blowing off a little bit of CO_2, is applied to the system, causing bubbles in the flow. Cooling down the water first before adding CO_2 has the same effect, for the same reason.

The produced hydrates that are injected with the slurry in the vessels tend to agglomerate on the surface of the water in the vessels. Filling the water in the vessels before the experiments to a level that is higher than the injection point results in better mixing, but still lumps of hydrates can be observed. After some minutes of producing hydrates, the suction line of the pump plugged in almost all conducted experiments, apparently caused by a lump of hydrates in the outlet of the vessel.

This does however not prevent samples from being taken, for which in all cases the valve in the suction line of the pump is used (see section 4-1-2). The slurry is pressed through a flexible tube connected to the outlet and run through a sieve with a bucket below to collect the liquid water. The sieve separates the hydrates from the liquid water and is placed in a clamp, which in turn is placed on a balance, allowing measurement of the hydrate mass. This is not done frequently enough to give a significant number, but was always in the order of magnitude of 200 gram hydrates per vessel.

4-4 Discussion

The density of the $H_2O - CO_2$ solution is modeled using the liquid phase CO_2 fraction from the flash calculation. The calculated values are compared with the measured values from the experimental set-up in figure 4-8(a). The corresponding experimental pressure, used as an input for the model, is presented in figure 4-8(b).

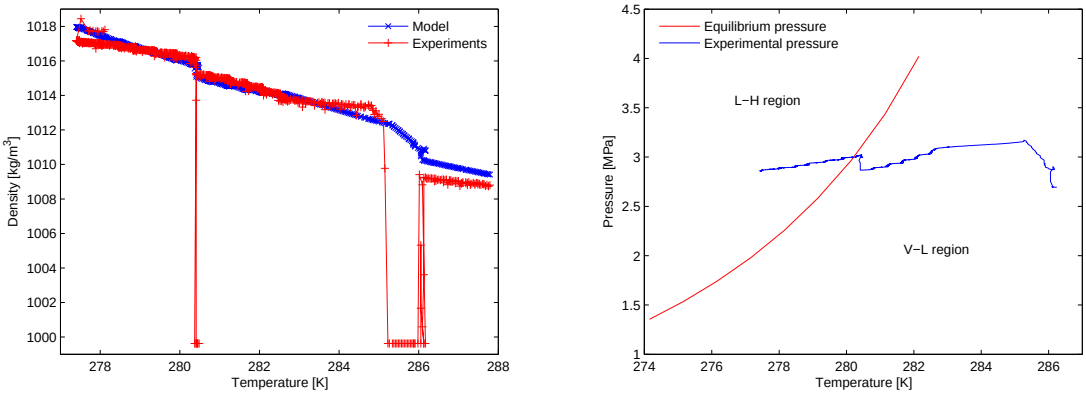

(a) Density.

(b) Pressure.

Figure 4-8: The predicted $H_2O - CO_2$ solution density compared with the measured density in figure 4-8(a) at the experimental pressures and temperatures in figure 4-8(b).

The red line in figure 4-8(b) represents the three phase equilibrium of water-rich liquid, hydrate and vapor. The pressure and temperature of the equilibrium curve marks the limits of hydrate formation. At higher temperature or lower pressures, hydrates cannot form and the system will contain only aqueous and CO_2 fluid phases. Hydrate formation can occur only to the left of equilibrium curve. In this case, hydrates start forming at the temperature of 277.5 K. At this temperature, the mole fraction of CO_2 dissolved in the bulk water phase is 2.6% and the mole fraction CO_2 at the interface is 2%. Then the driving force is 0.6%.

The figure clearly indicates large driving forces for mass transfer at these conditions which correspond to a driving force of 2.5 K. The discontinuity of the measured pressure in figure 4-8(b) indicates when CO_2 is added to the system and the pressure increases. This is also visible in the density measurements in figure 4-8(a), as gas bubbles present in the flow will disturb the density measurement.

At the lower temperatures (in the vapor-liquid region), the modeled solution density is higher than the measured values from the set-up. This might be caused by the calculated mole fractions from the flash calculation, which deviate from values in literature, as discussed in section 3-6. The lower predicted mole fraction results in a lower predicted molar volume of the solution and thus a higher density. This can be observed when the solution becomes supersaturated and the predicted density line crosses the experimental density. This deviation in the solution density will influence the calculation of the slurry density (see equation 3-56).

In figure 4-9 the temperatures and pressures of an experiment are presented. The point after which the solution becomes supersaturated is indicated with a vertical and horizontal red

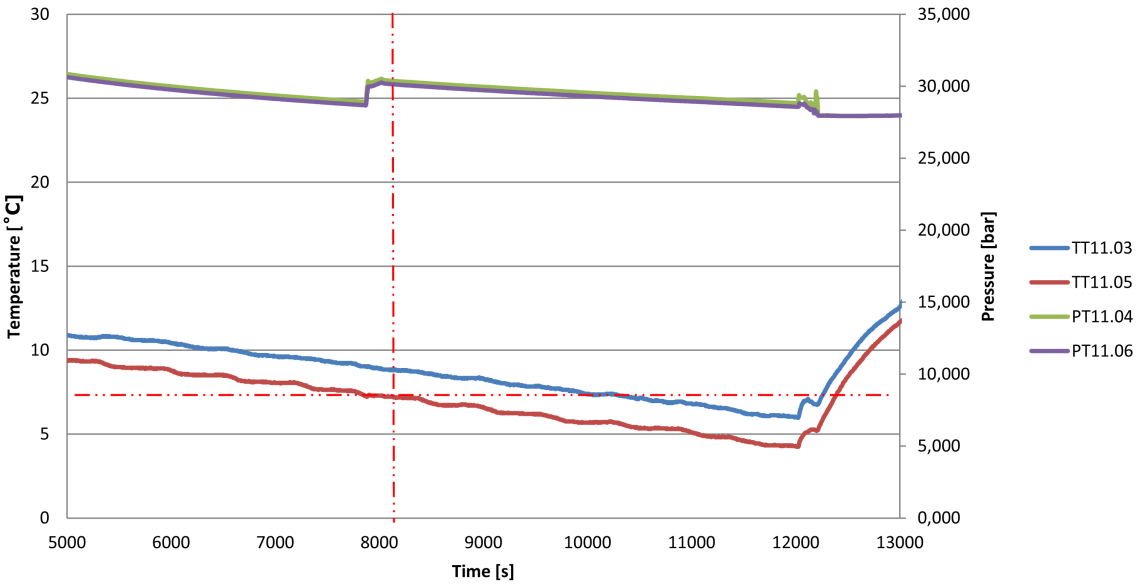

Figure 4-9: Temperatures and pressures from the experiment, corresponding with the density measurements in figure 4-10. Below the horizontal and left of the vertcial dashed line, the solution is supersaturated.

line. In figure 4-10 the measured density is presented as a function of time and compared with the predicted density.

As can be seen in figure 4-10, the measured density of the solution corresponds reaonable with the predicted density when the mixture is still in the vapor-liquid region, but as soon as the solution is supersaturated, the predicted density starts to increase and deviates more from the measured value. The discontinuity in the measured density is caused by the filling of CO_2 during the experiment, which results in gas bubbles in the flow. Neglecting the discontinuity in the density measurements, The relative error between measured and predicted density is within 0.08% and the absolute error within 0.8 kg/m^3.

Again in figure 4-10 a similar peak in the measured density is observed as in figure 4-7, but the density does not show a constant increase. As plugging occurred in one of the heat exchangers, the temperature was increased at the end of this experiment to dissociate the hydrates. This results in a decreasing density, as less CO_2 can be dissolved in water at higher temperatures.

The developed set-up is able to produce hydrates, although it is difficult to maintain a constant production. The coil heat exchangers are easily plugged when the mixture is cooled too fast or when the driving force is too large before the first hydrates form. Nevertheless a sample can be taken which can be used for experiments with meat.

The temperature transmitters in the set-up are connected in a 2-wire configuration, causing a much higher measurement error than when a 4-wire configuration is used. The pressure transmitters can be calibrated with a dead-weight tester to increase their accuracy for future measurements. The thermostatic baths used in the set-up are a bit unstable and sometimes suddenly switch to heating instead of cooling. Also the temperature of one of the baths

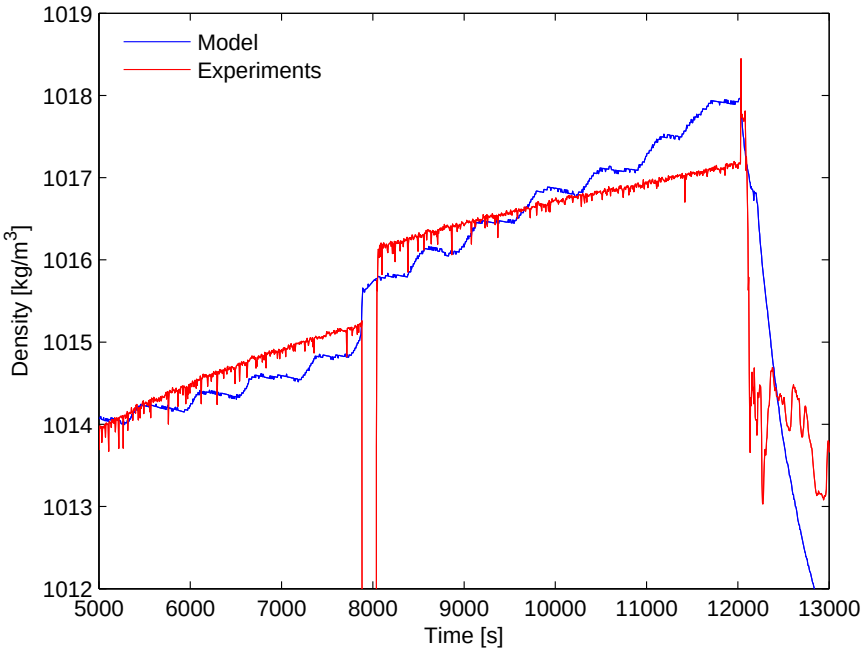

Figure 4-10: Measured density compared with the predicted solution density.

has a small overshoot before it stabilizes. The baths need to be watched constantly during experiments. These problems might be solved by maintenance of the thermostatic baths.

When hydrates are visible in the sight glasses, the measured density doesn't change, although sometimes a small peak is observed when the first hydrates are visible. This means that future predictions from a growth model can't be compared with the data measured in the current configuration of the experimental set-up.

Chapter 5

Conclusions and recommendations

5-1 Conclusions

1. A thermodynamic model has been developed to predict the pressure as a function of temperature in the hydrate forming region of $H_2O - CO_2$ mixture. The binary energy parameters in the UNIQUAC model, which is used to model the fluid phases of the $H_2O - CO_2$ mixture, have been regressed from equilibrium data by fitting the fugacities of the liquid and vapor phase to experimental data.

2. The thermodynamic model has been validated at equilibrium conditions with experimental data from literature. The equilibrium pressure is predicted by the developed model with an average absolute deviation of 0.084 MPa and a relative deviation between 0.15 and 4.42% compared to the experimental data given by [Wendland et al., 1999].

3. A flash model has been developed to predict the mole fractions of the components in the present phases. This model has been validated by comparing the CO_2 mole fraction in the liquid phase with the solubility of CO_2 in H_2O given by [Diamond and Akinfiev, 2003]. At equilibrium conditions these are in good agreement, but in the hydrate-liquid region the model predicts a lower value of the mole fraction compared to [Diamond and Akinfiev, 2003]. At a driving force of 2 K, the relative error is between 4.2 and 8.0 %.

4. The thermodynamic model should be improved further to predict the driving force needed for the growth model. The fugacity of H_2O in the hydrate phase is calculated using the cavity occupancy. These are calculated using the fugacity of CO_2 in the vapor phase instead of the hydrate phase. The developed model does not converge when the hydrate phase fugacity of CO_2 is used. This results in incorrect prediction of the fugacity coefficients used in the flash model and therefore incorrect prediction of the mole fractions in the hydrate-liquid region.

5. Experiments have been performed with a developed set-up to find the suitable conditions and operating procedure for hydrate formation. Hydrates are produced and samples of the slurry can be taken, so it is possible to perform experiments with meat. The

measured density however, does not show the expected reported in literature, when hydrates are visible in the sight glasses.

6. Density measurements from the experiments are compared with predicted $H_2O - CO_2$ solution densities. The trends are in good agreement, but as soon as the solution becomes supersaturated, the deviation increases. This is a direct result from the deviations of the mole fractions predicted by the flash model in the hydrate-liquid region.

5-2 Recommendations

1. It is recommended to improve the approximation of the binary interaction parameters u_{ij} in the calculation of the pressure and fugacities.

2. Improve the thermodynamic model by using the hydrate phase CO_2 fugacity in the calculation of the H_2O hydrate fugacity. This will allow a correct calculation of the solution density and, when the growth model is implemented, of the slurry density.

3. Incorporate the thermal energy released with hydrate formation to the bulk phase around the particle and the thermal energy extracted from the solution by the thermostatic baths in the model.

4. The accuracy of the temperature measurements could be improved by replacing the 2-wire temperature transmitters by 4-wire transmitters.

5. Get accurate measurements of the density by using either another method of the density measurement or by relocating the flow meter.

6. To prevent agglomeration of the hydrates, which may cause plugging of the outlet of the vessels, it is recommended to improve the mixing of the hydrate slurry in the vessels. This could be done by installing a (magnetic) mixer.

7. Investigate the influence of the flow rate during the experiments. The heat transfer in the thermostatic bath from the heat transfer fluid to the $H_2O - CO_2$ solution will be affected by the mass flow rate.

8. Determine the energy consumption of the system per unit of mass of cooled meat and compare that with the energy consumption of conventional cooling techniques. This will give a better understanding of the competitiveness of cooling with hydrates. It will also allow an economical assessment.

9. Develop a crystal growth model to predict the amount of hydrates formed in the coil heat exchangers of the experimental set-up, using the tools developed in the present study.

Bibliography

S. Adisasmito, R. J. Frank, and E. D. Sloan. Hydrates of carbon dioxide and methane mixtures. *Journal of Chemical & Engineering Data*, 36(1):68–71, 1991.

R. Barrer. Validity of clapeyron's equation for phase equilibria involving hydrates. *Nature*, 183(463), 1959.

P. R. Bishnoi and V. Natarajan. Formation and decomposition of gas hydrates. *Fluid Phase Equilibria*, 117(1-2):168–177, 1996.

I. Chatti, A. Delahaye, L. Fournaison, and J.-P. Petitet. Benefits and drawbacks of clathrate hydrates: a review of their areas of interest. *Energy Conversion and Management*, 46(9-10): 1333–1343, 2005.

M.-K. Chun and H. Lee. Kinetics of formation of carbon dioxide clathrate hydrates. *Korean Journal of Chemical Engineering*, 13(6):620–626, 1996.

M. A. Clarke and P. R. Bishnoi. Determination of the intrinsic kinetics of CO_2 gas hydrate formation using in situ particle size analysis. *Chemical Engineering Science*, 60(3):695–709, 2005.

W. A. Cole and G. Stephen P. Flash calculations for gas hydrates: A rigorous approach. *Chemical Engineering Science*, 45(3):569–573, 1990.

W. Davidson, D., R. Gough, S., P. Handa, Y., I. Ratcliffe, C., A. Ripmeester, J., and S. Tse, J. Some structural studies of clathrate hydrates. *J. Phys. Colloques*, 48(C1):537–542, 1987.

A. Delahaye, L. Fournaison, S. Marinhas, I. Chatti, J.-P. Petitet, D. Dalmazzone, and W. Fürst. Effect of thf on equilibrium pressure and dissociation enthalpy of CO_2 hydrates applied to secondary refrigeration. *Industrial & Engineering Chemistry Research*, 45(1):391–397, 2005.

A. Delahaye, L. Fournaison, S. Marinhas, and M. C. Martínez. Rheological study of CO_2 hydrate slurry in a dynamic loop applied to secondary refrigeration. *Chemical Engineering Science*, 63(13):3551–3559, 2008.

L. W. Diamond and N. N. Akinfiev. Solubility of CO_2 in water from -1.5 to 100 °C and from 0.1 to 100 MPa: evaluation of literature data and thermodynamic modelling. *Fluid Phase Equilibria*, 208(1-2):265–290, 2003.

Z. Duan, J. Hu, D. Li, and S. Mao. Densities of the CO_2 - H_2O and CO_2 - H_2O - $NaCl$ systems up to 647 K and 100 MPa. *Energy & Fuels*, 22(3):1666–1674, 2008.

P. Englezos and P. R. Bishnoi. Gibbs free energy analysis for the supersaturation limits of methane in liquid water and the hydrate-gas-liquid water phase behavior. *Fluid Phase Equilibria*, 42(0):129–140, 1988.

P. Englezos, N. Kalogerakis, P. D. Dholabhai, and P. R. Bishnoi. Kinetics of formation of methane and ethane gas hydrates. *Chemical Engineering Science*, 42(11):2647–2658, 1987.

L. Fournaison, A. Delahaye, I. Chatti, and J.-P. Petitet. CO_2 hydrates in refrigeration processes. *Industrial & Engineering Chemistry Research*, 43(20):6521–6526, 2004.

D. Glew. Some stoichiometric gas hydrates. *Nature*, 184(545), 1959.

N. Gnanendran and R. Amin. Modelling hydrate formation kinetics of a hydrate promoter - water - natural gas system in a semi-batch spray reactor. *Chemical Engineering Science*, 59 (18):3849–3863, 2004.

C. S. Grolleman. Projectplan fase 1 direct product koelen met CO_2 hydraten, 2010.

J. S. Gudmundsson, M. Parlaktuna, O. I. Levik, and V. Andersson. Laboratory for continuous production of natural gas hydrates. *Annals of the New York Academy of Sciences*, 912(1): 851–858, 2000.

A. K. Gupta, P. Raj Bishnoi, and N. Kalogerakis. A method for the simultaneous phase equilibria and stability calculations for multiphase reacting and non-reacting systems. *Fluid Phase Equilibria*, 63(1-2):65–89, 1991.

D. Hartono. Thermodynamic modeling of CO_2-tetrahydrofuran-water hydrates. Technical report, Delft University of Technology, 2011.

R. Heinemann, D. Da-Teh Huang, J. Long, and R. Saeger. Process for making gas hydrates, February 22, 2000 2000.

J. M. Herri, F. Gruy, J. S. Pic, M. Cournil, B. Cingotti, and A. Sinquin. Interest of in situ turbidimetry for the characterization of methane hydrate crystallization: Application to the study of kinetic inhibitors. *Chemical Engineering Science*, 54(12):1849–1858, 1999.

A. Hoffmann. Predictive model for hydrate formation in a tube-in-tube coil heat exchanger. Technical report, Delft University of Technology, January 2011 2011.

J. Hu, O. Sari, C. Mahmed, R. Cereghetti, and P. Homsy. Experimental study on flow behaviours of CO_2 hydrate slurry. In *Phase-Change Materials and Slurries for Refrigeration and Air Conditioning*, volume 5 of *Refrigeration Science and Technology*, pages 69–79. International Institute of Refrigeration.

J. Hu, O. Sari, C. Mahmed, R. Cereghetti, and P. Homsy. Experimental study on flow behaviours of CO_2 hydrate slurry, 2010.

J. Hu, P. Stéphane, O. Sari, and D. Lakehal. Experimental study on CO_2 gas hydrate cold storage, 2011.

S. P. Kang, H. Lee, and B. J. Ryu. Enthalpies of dissociation of clathrate hydrates of carbon dioxide, nitrogen, (carbon dioxide + nitrogen), and (carbon dioxide + nitrogen + tetrahydrofuran). *The Journal of Chemical Thermodynamics*, 33(5):513–521, 2001.

H. C. Kim, P. R. Bishnoi, R. A. Heidemann, and S. S. H. Rizvi. Kinetics of methane hydrate decomposition. *Chemical Engineering Science*, 42(7):1645–1653, 1987.

J. B. Klauda and S. I. Sandler. A fugacity model for gas hydrate phase equilibria. *Industrial & Engineering Chemistry Research*, 39(9):3377–3386, 2000.

B. Kvamme, A. Graue, E. Aspenes, T. Kuznetsova, L. Granasy, G. Toth, T. Pusztai, and G. Tegze. Kinetics of solid hydrate formation by carbon dioxide: Phase field theory of hydrate nucleation and magnetic resonance imaging. *Physical Chemistry Chemical Physics*, 6(9):2327–2334, 2004.

M. J. Lazzaroni, D. Bush, R. Jones, J. P. Hallett, C. L. Liotta, and C. A. Eckert. High-pressure phase equilibria of some carbon dioxide-organic-water systems. *Fluid Phase Equilibria*, 224 (1):143–154, 2004.

S. Marinhas, A. Delahaye, L. Fournaison, D. Dalmazzone, W. Fürst, and J.-P. Petitet. Modelling of the available latent heat of a CO_2 hydrate slurry in an experimental loop applied to secondary refrigeration. *Chemical Engineering and Processing*, 45(3):184–192, 2006.

M. L. Michelsen. Calculation of hydrate fugacities. *Chemical Engineering Science*, 46(4): 1192–1193, 1991.

A. Mills. *Basic Heat & Mass Transfer*. Prentice Hall, Inc., 2nd edition, 1999.

J. Munck, S. Skjold-Jørgensen, and P. Rasmussen. Computations of the formation of gas hydrates. *Chemical Engineering Science*, 43(10):2661–2672, 1988.

V. Natarajan, P. R. Bishnoi, and N. Kalogerakis. Induction phenomena in gas hydrate nucleation. *Chemical Engineering Science*, 49(13):2075–2087, 1994.

V. Ness, J. Smith, and M. M. V. Ness. *Introduction to Chemical Engineering Thermodynamics*. McGraw-Hill Education Europe, 7th edition, 2005.

H. Orbey and S. I. Sandler. On the combination of equation of state and excess free energy models. *Fluid Phase Equilibria*, 111(1):53–70, 1995.

W. R. Parrish and J. M. Prausnitz. Dissociation pressures of gas hydrates formed by gas mixtures. *Industrial & Engineering Chemistry Process Design and Development*, 11(1): 26–35, 1972.

C. P. Ribeiro Jr and P. L. C. Lage. Modelling of hydrate formation kinetics: State-of-the-art and future directions. *Chemical Engineering Science*, 63(8):2007–2034, 2008.

K. Sabil. *Phase behaviour, thermodynamics and kinetics of clathrate hydrate systems of carbon dioxide in presence of thetrahydrofuran and electrolytes*. Phd thesis, 2009.

P. Skovborg and P. Rasmussen. A mass transport limited model for the growth of methane and ethane gas hydrates. *Chemical Engineering Science*, 49(8):1131–1143, 1994.

E. Sloan and C. Koh. *Clathrate hydrates of natural gases.* CRC Press, 2008.

E. D. Sloan. Clathrate hydrates:the other common solid water phase. *Industrial & Engineering Chemistry Research*, 39(9):3123–3129, 2000.

E. D. Sloan and F. Fleyfel. Hydrate dissociation enthalpy and guest size. *Fluid Phase Equilibria*, 76:123–140, 1992.

D. F. Spencer and W. J. North. Method for the production of carbon dioxide hydrates, 1996.

S. Takeya, A. Hori, T. Hondoh, and T. Uchida. Freezing-memory effect of water on nucleation of CO_2 hydrate crystals. *The Journal of Physical Chemistry B*, 104(17):4164–4168, 2000.

H. Teng, A. Yamasaki, and Y. Shindo. Stability of the hydrate layer formed on the surface of a CO_2 droplet in high-pressure, low-temperature water. *Chemical Engineering Science*, 51(22):4979–4986, 1996.

J. H. Van Der Waals and J. C. Platteeuw. Validity of clapeyron's equation for phase equilibria involving clathrates. *Nature*, 183(4659):462–462, 1959a. 10.1038/183462a0.

J. H. Van Der Waals and J. C. Platteeuw. Clathrate solutions. *Advances in Chemical Physics*, 2:57, 1959b.

VDI. Warmeatlas, 1997.

A. Vysniauskas and P. R. Bishnoi. A kinetic study of methane hydrate formation. *Chemical Engineering Science*, 38(7):1061–1072, 1983.

M. Wendland, H. Hasse, and G. Maurer. Experimental pressure - temperature data on three- and four- phase equilibria of fluid, hydrate, and ice phases in the system carbon dioxide - water. *Journal of Chemical & Engineering Data*, 44(5):901–906, 1999.

D. Yang, L. A. Le, R. J. Martinez, R. P. Currier, D. F. Spencer, and G. Deppe. Heat transfer during CO_2 hydrate formation in a continuous flow reactor. *Energy & Fuels*, 22 (4):2649–2659, 2008.

S. O. Yang, I. M. Yang, Y. S. Kim, and C. S. Lee. Measurement and prediction of phase equilibria for water+CO_2 in hydrate forming conditions. *Fluid Phase Equilibria*, 175(1-2): 75–89, 2000.

Appendix A

Cooling of meat

In this appendix the heat transfer in the experimental set-up as described in chapter 4 is determined in section A-1. Using the heat transfered to the $H_2O - CO_2$ mixture, the amount of hydrates that can be produced per unit of time is calculated in section A-2. This is done under the assumption that the whole cooling power is used to remove the heat of formation of the hydrates.

A-1 Heat transfer

All dimensionless numbers, thermodynamic properties and correlation in this section are taken from Mills [Mills, 1999], section 4.3 and 4.4.

The heat transfer in thermostatic bath 1 where the hydrates are formed in a coil, can be described by

$$Q = U \cdot A \cdot (T_{sol} - T_b) \tag{A-1}$$

With

$$\frac{1}{U} = \frac{1}{h_o} + \frac{d_o \cdot \ln(\frac{d_o}{d_i})}{2 \cdot k_w} + \frac{d_o}{d_i \cdot h_i} \tag{A-2}$$

The inside diameter $d_i = 6\,mm$ and the outside diameter $d_o = 8\,mm$. The coil has $n_w = 12$ circular windings with a diameter of $d_w = 125\,mm$ in the thermostatic bath, giving a length of

$$L = 2 \cdot \pi \cdot \frac{d_w}{2} \cdot n_w = 2 \cdot \pi \cdot \frac{125 \cdot 10^{-3}}{2} \cdot 12 = 4.71\,m \tag{A-3}$$

And a heat exchanger area on the outside of the tube

$$A_o = 2 \cdot \pi \cdot r_o \cdot L = 2 \cdot \pi \cdot \frac{8 \cdot 10^{-3}}{2} \cdot 3.77 = 0.12\,m^2 \tag{A-4}$$

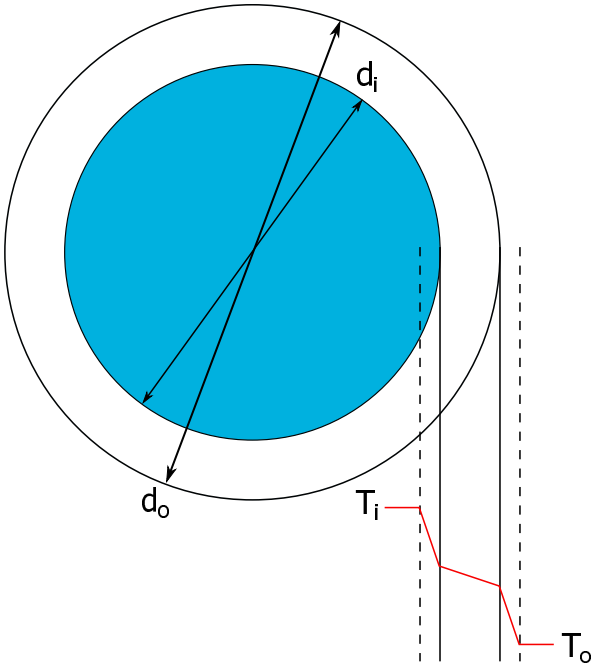

Figure A-1: Heat transfer in a tube

Heat transfer through the wall

Heat is conducted through the metal wall, using a thermal conductivity coefficient of $k_m = 15\ \frac{W}{m \cdot K}$. The temperature of the wall is assumed to be the average of the hydrate forming mixture temperature (8 °C) and the bath temperature (0 °C).

$$T_{wall} = \frac{T_{solution} + T_b}{2} = \frac{279.15 + 273.15}{2} = 276.15\ K \tag{A-5}$$

Heat transfer on the outside of the tube

Heat is transfered from the thermostatic bath to the hydrate forming mixture in the tubes by natural convection. Using

$$\beta = 1.16 \cdot 10^{-6}\ \frac{1}{K}$$

$$g = 9.81\ m/s^2$$

$$\Delta T = T_{wall} - T_b = 276.15 - 273.15 = 3\ K$$

$$\alpha = \frac{k}{\rho \cdot c_p} = \frac{0.553}{1000 \cdot 4210} = 1.31 \cdot 10^{-7}\ m^2/s$$

$$d_o = 8 \cdot 10^{-3}\ m$$

$$\nu = 1.8 \cdot 10^{-6}\ m^2/s$$

and

$$Ra_D = \frac{\beta \cdot \Delta T \cdot g \cdot d_o^3}{\nu \cdot \alpha} = \frac{1.16 \cdot 10^{-6} \cdot 3 \cdot 9.81 \cdot (8 \cdot 10^{-3})^3}{1.8 \cdot 10^{-6} \cdot 1.31 \cdot 10^{-7}} = 74.3 \tag{A-6}$$

For a $Ra_D \lesssim 10^9$, the Nusselt number can be described by

$$Nu_D = 0.36 + \frac{0.518 \cdot Ra_D^{1/4}}{\left[1 + (0.559/Pr)^{9/16}\right]^{4/9}} = 0.36 + \frac{0.518 \cdot 74.3^{1/4}}{\left[1 + (0.559/13.67)^{9/16}\right]^{4/9}} = 1.78 \tag{A-7}$$

the heat transfer coefficient for natural convection is given by

$$h_o = \frac{k}{d_o} Nu_D = \frac{0.553}{8 \cdot 10^{-3}} \cdot 1.78 = 123.1 \, \frac{W}{m^2 \cdot K} \tag{A-8}$$

Heat transfer on the inside of the tube

Heat transfer from the metal wall to the hydrate forming slurry is done by forced convection. Using

$$Pr = \frac{C_p \cdot \mu}{k} = \frac{4217 \cdot 14 \cdot 10^{-4}}{0.556} = 10.6 \tag{A-9}$$

$$Re_D = \frac{\rho \cdot u \cdot d_i}{\mu} = \frac{1000 \cdot 1 \cdot 6 \cdot 10^{-3}}{14 \cdot 10^{-4}} = 4286 \tag{A-10}$$

For a spiral tube the critical Reynolds number is given by

$$Re_{crit} = 2300 \left[1 + 8.6 \cdot \left(\frac{d}{D}\right)^{0.45}\right] = 2300 \left[1 + 8.6 \cdot \left(\frac{6 \cdot 10^{-3}}{0.125}\right)^{0.45}\right] = 7344 \tag{A-11}$$

For $Re_D \leqslant Re_{crit}$, the Nusselt number is given by [VDI, 1997]

$$Nu = \left(3.66 + 0.08 \left[1 + 0.8 \left(\frac{d}{D}\right)^0 .9\right] \cdot Re^m \cdot Pr^{1/3}\right) \cdot \left(\frac{Pr}{Pr_w}\right)^{0.14} \tag{A-12}$$

With

$$m = 0.5 + 0.2903 \cdot \left(\frac{d}{D}\right)^{0.194} = 0.5 + 0.2903 \cdot \left(\frac{6 \cdot 10^{-3}}{0.125}\right)^{0.194} = 0.66 \tag{A-13}$$

Giving a Nusselt number of

The heat transfer coefficient on the inside of the tube is given by

$$h_i = \frac{Nu \cdot k}{d_i} = \frac{49.6 \cdot 0.556}{6 \cdot 10^{-3}} = 4592.3 \, \frac{W}{m^2 \cdot K} \tag{A-14}$$

Overall heat transfer coefficient

Assuming the temperature difference of the hydrate mixture is 5 K and the mixture is cooled down to 8 °C (mean temperature is 10.5 °C) and a constant thermostatic bath temperature of 0 °C, this results in a heat flux of

$$\frac{1}{U} = \frac{1}{123.1} + \frac{8 \cdot 10^{-3} \cdot \ln(\frac{8 \cdot 10^{-3}}{6 \cdot 10^{-3}})}{2 \cdot 15} + \frac{8 \cdot 10^{-3}}{6 \cdot 10^{-3} \cdot 4592.3} = 0.008 \, \frac{m^2 \cdot K}{W} \tag{A-15}$$

Which gives an overall heat transfer coefficient $U = 117.8 \, \frac{W}{m^2 \cdot K}$

$$Q = U \cdot A \cdot (T_{sol} - T_{wall}) = 117.8 \cdot 0.12 \cdot (279.15 - 277.15) = 41.8 \, W \tag{A-16}$$

A-2 Cooling of meat

Hydrates have an enthalpy of dissociation of about 500 kJ/kg and with the thermal energy transmitted known, the amount of hydrates can be calculated, assuming al heat is used for the hydrate production.

$$\frac{0.0418\ \frac{kJ}{s}}{500\ \frac{kJ}{kg}} = 8.4 \cdot 10^{-5}\ kg/s = 0.084\ g/s \tag{A-17}$$

The total mass flow in the system will be approximately 100 dm^3/hr, and using a density of 1000 kg/m^3 this is a mass flow of 0.028 kg/s.

Using a density of and $\rho_w = 1000\ kg/m^3$ for water and $\rho_H = 1040\ kg/m^3$ for hydrates , the solid fraction (hydrates) is given by

$$w_s = 1 - \frac{\dot{m}_H}{\dot{m}_w + \dot{m}_H} = 1 - \frac{8.4 \cdot 10^{-5}}{8.4 \cdot 10^{-5} + 0.028} = 0.003 \tag{A-18}$$

Assuming a water fraction of 74 % in meat that has to be cooled from 25 °C to 8 °C, 65 $\frac{kJ}{kg}$ is needed.

$$\dot{m}_{meat} = \frac{Q}{\Delta h_{meat}} = \frac{\dot{m}_H \cdot \Delta h_{diss}}{\Delta h_{meat}} = \frac{8.4 \cdot 10^{-5} \cdot 500}{65} = 0.65\ g/s \tag{A-19}$$

or 1 kg of meat can be cooled in 1547 seconds.

The sample volume of $4.9 \cdot 10^{-4}\ m^3$ has a mass of

$$m_{sol}^{sample} = V_{sample} \cdot \rho_{solution} = 4.9 \cdot 10^{-4} \cdot 1015 = 0.49\ kg \tag{A-20}$$

using ρ_{sol} =1015 kg/m^3.

The mass of hydrates in the sample is

$$m_H^{sample} = w_H \cdot m_{sol}^{sample} = 0.003 \cdot 0.49 = 1.5 \cdot 10^{-3}\ kg\ = 1.5\ g \tag{A-21}$$

and with that

$$m_{meat}^{sample} = \frac{m_H^{sample} \cdot \Delta h_H}{\Delta h_{meat}} = \frac{1.5 \cdot 10^{-3} \cdot 500}{65} = 11.5 \cdot 10^{-3}\ kg = 1.15\ g \tag{A-22}$$

meat can be cooled from 25 to 8 °C.

Appendix B

Model code

The Matlab code of the thermodynamic equilibrium model and the flash model are given in this chapter. The thermodynamic model is rewritten as a Matlab function for use in the flash model.

B-1 Matlab code flash model

```
1
2  v1=1/23;
3  v2=3/23;
4
5  flag=1;
6
7  NCO2=0.121;              %
8  %Temperature range in which the flash calculation is done
9  T=274.15:1:282.15;
10 t=length(T);
11
12 display=1;
13
14 %Number of components (1=CO2, 2=H2O)
15 NumC=2;
16 %Number of phases (1=vapor, 2=liquid, 3=hydrate)
17 NumP=3;
18 Xini=[0.1 0.5];
19 OPTIONS=optimset('Display','off','MaxIter',1000,'MaxFunEvals',10000);
20 z=[0.8 0.2];             %Overal mole fractions H2O-CO2 in the system
21
22
23 iter_max=500;            %maximum number of operations
24 tol=1e-4;                %tolerance condition
25
26 epsilon=1e-8;
```

```
27
28 %Initial fractions CO2 and H2O (v-l-h)
29 x=[0.9 0.015 0.05; 0.01 0.84 0.15];
30
31 %Initial value hydrate fraction
32 beta(3)=0.5;
33
34 %Calculate mole fractions for specified temperatures
35 for b=1:t
36     iter=0;
37     dif=1;
38     %Mole fraction CO2 dissolved in water (Diamond,2003), should be equal
39     %to calculated mole fraction CO2 in liquid phase
40     x_CO2(b)=(1.570415+7.887505*1e-2*(T(b)-273.15)+4.734722*1e-3*...
41         (T(b)-273.15)^2+4.56477*1e-4*(T(b)-273.15)^3-3.796084*1e-5*...
42         (T(b)-273.15)^4)*1e-2;
43
44     %Iterature until difference between mole fraction from current and
45     %previous calculated mole fraction is smaller than specified tolerance
46     %or until a maximum number of iterations has been reached
47     while ((dif > tol) && (iter < iter_max))
48
49
50         x_old=x;
51         %Count number of iterations
52         iter = iter + 1;
53
54         %Calculated fugacities and equilibrium pressure for specified
55         %temperature with equilibrium model
56         [fugH2O_h fcoefH2O_h fugCO2_l fugH2O_l fugCO2_v fugH2O_v...
57             fcoefCO2_l fcoefCO2_v fcoefH2O_l fcoefH2O_v fugCO2_h...
58             fcoefCO2_h P y_CO2 y_H2O x_H_CO2 x_H_H2O theta]=...
59             Func_eq(T(b), x(1,1), x(2,1), x(1,2) ,x(2,2));
60
61
62         %Calculate distribution coefficients
63         K_CO2_v=1;      %vapor phase is reference phase -> K_v=1
64         K_H2O_v=1;      %vapor phase is reference phase -> K_v=1
65
66         K_CO2_l=(fcoefCO2_v)/(fcoefCO2_l);
67         K_CO2_h=(fcoefCO2_v)/fcoefCO2_h;
68         K_H2O_l=(fcoefH2O_v)/(fcoefH2O_l);
69         K_H2O_h=(fcoefH2O_v)/(fcoefH2O_h);
70
71         K=[K_CO2_v K_CO2_l K_CO2_h; K_H2O_v K_H2O_l K_H2O_h];
72
73         %Objective function minimization
74         [X FVAL FLAG] = fsolve('obj_FlashMulti',[Xini],OPTIONS,z,K,...
75                         NumP,NumC,0);
76
77         %beta = phase fractions (1=v,2=l,3=h)
78         beta = zeros(NumP,1)';
79         %omega = stability criterium (1=v,2=l,3=h)
80         omega = zeros(NumP,1)';
81
82         for i = 2:NumP
83             if X(i-1) < 0
```

```
84                  alpha(i) = 0;
85                  omega(i) = -X(i-1);
86              else
87                  beta(i) = X(i-1);
88                  omega(i) = 0;
89              end
90          end
91
92          omega(1) = 0;
93          beta(1) = 1-sum(beta);
94          beta = abs(beta);
95
96          for i = 1:NumP
97              if ((beta(i) <= epsilon))
98                  beta(i) = 0;
99              end
100             if (omega(i) <= epsilon)
101                 omega(i) = 0;
102             end
103         end
104
105         beta = abs(beta)/sum(abs(beta));
106
107         for i = 2:NumP
108             if omega(i) > 0
109                 Xini(i-1) = -omega(i);
110             else
111                 Xini(i-1) = beta(i);
112             end
113         end
114
115         %Updating of compositions
116         for i = 1:NumC
117             sumat = 0;
118             for j = 2:NumP
119                 sumat = sumat + (K(i,j)*exp(omega(j)) - 1)*beta(j);
120             end
121             x(i,1) = z(i)/(1+sumat);
122         end
123
124         for i = 1:NumC
125             for j = 2:NumP
126                 x(i,j) = x(i,1)*K(i,j)*exp(omega(j));
127             end
128         end
129
130         for j = 1:NumP
131             sumat = sum(abs(x(:,j)));
132             for i = 1:NumC
133                 x(i,j) = abs(x(i,j))/sumat;
134             end
135         end
136
137
138         dif = 0;
139         for j = 1:NumP
140             for i = 1:NumC
```

```
141                 dif = dif + abs(x(i,j) - x_old(i,j));
142             end
143         end
144     end
145
146
147     for j = 1:NumP-1
148         if omega(j) == 0
149             for k = j+1:NumP
150                 if (abs(K(1,k) - K(1,j)) < 1e-3)
151                     beta(j) = beta(j) + beta(k);
152                     beta(k) = 0;
153                 end
154             end
155         end
156     end
```

B-2 Matlab code thermodynamic model

```
1  close all
2  clear all
3  clc
4
5  profile on
6
7  %Set constants and constant parameters for CO2 and H2O
8  Constants;
9  h = waitbar(0,'Please wait...');
10
11 %Maximum difference between fugacity of water in liquid phase and in
12 %hydrate phase
13 error = 1e1;
14
15
16 %Temperature range in which equilibrium pressure and other properties will
17 %be calculated
18 T=274.15:1:282.15;
19 t=length(T);
20
21
22
23 xH=0.8;
24
25 %molar  fraction  (vapor) -  initial  guess
26 y =  [0.95 0.05];
27
28
29 %Calculate equilibrium pressure for given temperature
30 for b=1:t
31     P=Pinit;
32     %Mole fraction CO2 dissolved in water (Diamond, 2003)
33     xCO2=(1.570415+7.887505*1e-2*(T(b)-273.15)+4.734722*1e-3*(T(b)-273.15)^2+...
34         4.56477*1e-4*(T(b)-273.15)^3-3.796084*1e-5*(T(b)-273.15)^4)*1e-2;
```

```
35
36      %Mole fraction H2O in liquid phase
37      xH2O=1-xCO2;
38      x =  [xCO2 xH2O];
39
40
41      %Initial value for fugacity difference of H2O in liquid phase and
42      %hydrate phase
43      ∆fug=3001;
44
45
46          %Iterate until ∆fug < error (and equilibrium pressure is
47          %obtained for temperature T
48          while  abs(∆fug) >  error
49
50              %P=P(b);
51              %UNIQUAC energy parameter, uij [J/mol]
52              uCO2H2O=-55720.3+279.8224*T(b);
53              uH2OCO2=-19599+78.13*T(b);
54              %tau [-] --> (Sabil eq. 7.23)
55              [tauCO2H2O tauH2OCO2 tauCO2CO2 tauH2OH2O]=Func_tau(uCO2H2O,...
56                                                      uH2OCO2,R,T(b));
57              %Peng-Robinson-Stryjek-Vera EoS parameters (a=attractive volume
58              %parameter [(kg*m^5)/(mol^2 * s^2)],b= excluded volume
59              %parameter [m^3/mol])
60              [aCO2 bCO2]=Func_ab(T(b), R, Tc(1), Pc(1), omega(1), K1(1));
61              [aH2O bH2O]=Func_ab(T(b), R, Tc(2), Pc(2), omega(2), K1(2));
62
63
64              %  LIQUID PHASE
65              %phi, volume fraction, liqiud
66              [phiCO2_l phiH2O_l]=Func_phi(r(1),r(2),x(1),x(2));
67              %theta, surface area fraction, liquid
68              [thetaCO2_l thetaH2O_l]=Func_theta(q(1),q(2),x(1),x(2));
69              %Excess Gibbs free energy liquid phase (GE/RT) [-]
70              GERT_l=Func_GERT(x(1),x(2),phiCO2_l,phiH2O_l,thetaCO2_l,...
71                  thetaH2O_l,tauCO2H2O,tauH2OCO2,tauCO2CO2,tauH2OH2O,...
72                  q(1),q(2),zcoord);
73              %Huron-Vidal-Orbey-Sandler (HVOS) mixing rule parameters
74              %(dimensionless) Abig [mol^2], Bbig [mol]
75              [Abig_l Bbig_l bmix_l]=Func_ABbig(x(1),x(2),aCO2,...
76                                  aH2O,bCO2,bH2O,R,T(b),P,GERT_l,Cstar);
77              %Calculate compressibility Z of liquid phase
78              %and molar volume
79              [Zliq Vliq Rho_liq]=Func_Z_l(Abig_l,Bbig_l,R,T(b),P);
80              %Activity coefficient liquid phase
81              [gammaCO2_l gammaH2O_l]=Func_act(x(1),x(2),phiCO2_l,...
82                                  phiH2O_l,thetaCO2_l,thetaH2O_l,...
83                                  q(1), q(2),tauCO2H2O,tauH2OCO2,...
84                                  tauCO2CO2,tauH2OH2O,zcoord,r(1),r(2));
85              %Fugacity liquid phase
86              [fcoefCO2_l fugCO2_l]=Func_fug(x(1),aCO2,bCO2,bmix_l,Bbig_l,...
87                                  gammaCO2_l,Zliq,R,P,T(b),Cstar);
88              [fcoefH2O_l fugH2O_l]=Func_fug(x(2),aH2O,bH2O,bmix_l,Bbig_l,...
89                                  gammaH2O_l,Zliq,R,P,T(b),Cstar);
90
91
```

```
92
93                  %VAPOR PHASE
94                  %Inital values for iteration variables
95                  Ysumold = 1;
96                  ΔYsum =0.1;
97                  %Iterate until sum of vapor mole fraction of two
98                  %sequential iteration steps is smaller than 0.01.
99                  %Caculation of thermodynamic properties is similar to
100                 %liquidphase.
101                 while abs(ΔYsum)>0.001
102                         %phi, volume fraction, vapour
103                         [phiCO2_v phiH2O_v]=Func_phi(r(1),r(2),y(1),y(2));
104                         %theta, surface area fraction, vapour
105                         [thetaCO2_v ...
                                thetaH2O_v]=Func_theta(q(1),q(2),y(1),y(2));
106                         %Excess Gibbs free energy vapour phase (GE/RT) [-]
107                         GERT_v=Func_GERT(y(1),y(2),phiCO2_v,phiH2O_v,...
108                                 thetaCO2_v,thetaH2O_v,tauCO2H2O,tauH2OCO2,...
109                                 tauCO2CO2,tauH2OH2O,q(1),q(2),zcoord);
110                         %Huron-Vidal-Orbey-Sandler (HVOS) mixing rule
111                         %parameters (dimensionless),Abig [mol^2], Bbig [mol]
112                         [Abig_v Bbig_v bmix_v]=Func_ABbig(y(1),y(2),aCO2,...
113                                                 aH2O,bCO2,bH2O,R,T(b),P,GERT_v,...
114                                                 Cstar);
115                         %Calculate compressibility Z of vapour phase
116                         %and molar volume
117                         [Zvap Vvap Rho_vap]=Func_Z_v(Abig_v,Bbig_v,R,T(b),P);
118                         %Activity coefficient vapour phase
119                         [gammaCO2_v ...
                                gammaH2O_v]=Func_act(y(1),y(2),phiCO2_v,...
120                                         phiH2O_v,thetaCO2_v,thetaH2O_v,q(1),...
121                                         q(2),tauCO2H2O,tauH2OCO2,tauCO2CO2,...
122                                         tauH2OH2O,zcoord,r(1),r(2));
123                         %Fugacity vapour phase
124                         [fcoefCO2_v fugCO2_v]=Func_fug(y(1),aCO2,bCO2,...
125                                                 bmix_v, Bbig_v, gammaCO2_v,...
126                                                 Zvap,R,P,T(b),Cstar);
127                         [fcoefH2O_v fugH2O_v]=Func_fug(y(2),aH2O,bH2O,...
128                                                    bmix_v,Bbig_v,gammaH2O_v,...
129                                                    Zvap,R,P,T(b),Cstar);
130                         %Calculate new vapor mole fractions
131                         [yCO2 yH2O Ysum]=Func_ynew(fcoefCO2_l,fcoefCO2_v,...
132                                                  fcoefH2O_l,fcoefH2O_v,x(1),x(2));
133                         y=[yCO2 yH2O];
134
135                         ΔYsum  = Ysumold-Ysum;
136                         Ysumold=Ysum;
137                         Ycontrol = yCO2+yH2O;
138                 end
139
140
141
142             %Fugacity of H2O in hydrate phase
143             [fugH2O_h fcoefH2O_h ΔmiuBL ΔmiuMTH x_H_CO2 x_H_H2O...
144                 theta1CO2 theta2CO2]=Func_fugH2Ohyd(gammaH2O_l,...
145                 x(2),P,T(b),Tref,fugCO2_v,R,xH);
146             %Fugacity of CO2 in hydrate phase
```

```
147             [fugCO2_h fcoefCO2_h]=Func_fugCO2h(T(b),P,x_H_CO2, x_H_H2O);
148
149
150             %Fugacit difference between H2O in liquid phase and hydrate
151             %phase (should be equal in equilibrium)
152             ∆fug=fugH2O_l-fugH2O_h;
153
154             %Calculate new pressure
155             P=P+abs(∆fug);
156
157
158         end
159
160
161
162         %Store variables for plotting
163         %Fugacities
164         fCO2Lplot(b)=fugCO2_l;
165         fH2OLplot(b)=fugH2O_l;
166         fCO2vplot(b)=fugCO2_v;
167         fH2Ovplot(b)=fugH2O_v;
168         fugCO2_hplot(b)=fugCO2_h;
169         fH2Ohydplot(b)=fugH2O_h;
170
171         %Fugacity coefficients
172         fcoefCO2lplot(b)=fcoefCO2_l;
173         fcoefH2O_lplot(b)=fcoefH2O_l;
174         fcoefCO2_hplot(b)=fcoefCO2_h;
175
176         %Pressure and temperature
177         Pplot(b)=P*1e-6;
178         Tplot(b)=T(b);
179
180         %Update waitbar
181         waitbar(b/t,h,sprintf('Progress...'));
182
183 end
184
185 %Plot calculated equilibrium pressure and fugacities
186 plotequilibriumP
187
188
189 %Delete waitbar
190 delete(h)
191 profile viewer
```